NUMERICAL MODELING FOR ORTHOGONAL CUTTING OF BRITTLE MATERIALS

A Dissertation

by

BEHROUZ TAKABI

Submitted to the Office of Graduate and Professional Studies of
Texas A&M University
in partial fulfillment of the requirements for the degree of

DOCTOR OF PHILOSOPHY

Chair of Committee, Bruce Tai
Committee Members, Robert Lytton
Alan Freed
Harry Hogan
Head of Department, Andreas A. Polycarpou

May 2019

Major Subject: Mechanical Engineering

ABSTRACT

Brittle materials include a wide range of materials such as bones, ceramics, and minerals. Machining brittle materials with precision is crucial in the manufacturing of devices for a wide range of industries from medical instrument manufacturers to aerospace industry. However, the models of brittle materials cutting are not yet well-established. The difficulty of modeling such a process can be attributed to the crack initiation and propagation governed by fracture mechanism. A brittle cutting generally produces powder-like chips, fragmented and dusty debris, which can be hardly captured by common numerical models such as finite element method (FEM). To address the issue, this study investigates two different methods to model brittle materials cutting; smoothed particle hydrodynamics (SPH) and embedded cohesive zone finite element method (ECZ-FEM). SPH, which is lagrangian method, can be an alternative option because of the particle-based algorithm eliminating the use of volumetric elements. The current research investigates the effects of particle density and damage criteria on the chip morphology and cutting force. The natural separation of particles and numerical instabilities hinder the application of SPH for brittle cutting and it needs further study. Besides, this research proposes a fracture-based finite element model, ECZ-FEM, which does not require predefined crack path. In ECZ-FEM, a network of cohesive zone (CZ) elements is embedded in the material body which potentially gives the model the ability to capture undetermined fracture during a cutting process. In terms of chip morphology, ECZ-FEM is able to capture dusty debris, irregular chips, and unstable crack propagation as expected for brittle materials cuttings.

The model, though, overestimates the average cutting forces by 30-50% and shows a more oscillating force profile. The key to build a successful model is selecting an appropriate scaling factor, *f*, acquired by model calibration against the experiment. Experiments is carried out for orthogonal cutting of bone-mimetic materials. ECZ-FEM seems like a good method to model the cutting of tough and stiff brittle materials with no plastic deformation.

ACKNOWLEDGEMENTS

I would like to thank my advisor, Dr. Bruce Tai, for his subtle comments and time on our long discussions which have improved the quality of my research and papers.

I would also like to thank my committee members, Dr. Robert Lytton, Dr. Harry Hogan and Dr. Alan Freed for their guidance and support throughout the course of this research.

Finally, thanks to my mother and father for their encouragement.

CONTRIBUTORS AND FUNDING SOURCES

This work was supervised by a dissertation committee consisting of Professor Bruce Tai and Professors Alan Freed and Harry Hogan of the Department of Mechanical Engineering and Professor Robert Lytton of Department of Civil Engineering. All work for the dissertation was completed independently by the student.

TABLE OF CONTENTS

LIST OF FIGURES

LIST OF TABLES

1. INTRODUCTION

1.1. Background

Machining is the main process for manufacturing of devices for different industries, including semiconductor, optical communication, computer peripherals, medical, automotive and aerospace. Hard and brittle materials such as glasses, engineering and functional ceramics are one of the most difficult materials to machine [1].

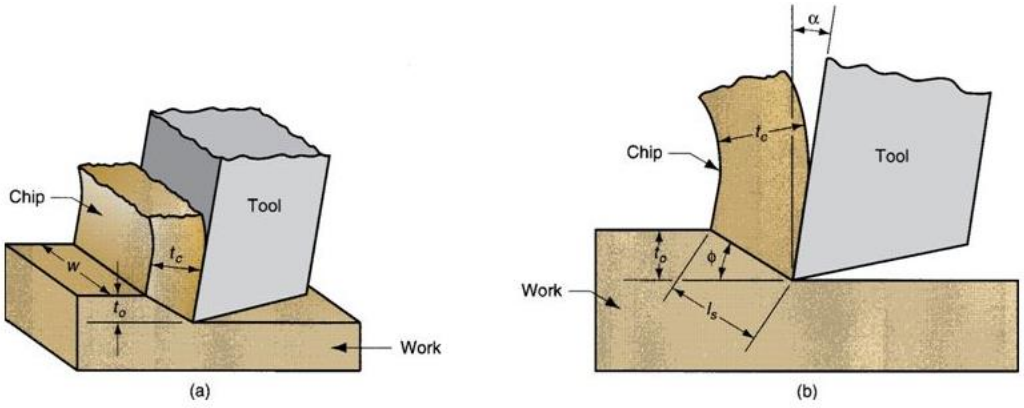

Figure 1-1. (a) 3D and (b) 2D schematics of orthogonal cuttings

Orthogonal cutting, as shown in Figure 1-1, is the basic configuration of all machining processes to describe the interaction between the cutting tool and work-material. This cutting concept has been applied to a variety of fields from traditional metal alloys, brittle ceramics, to non-engineering materials such as rocks and human tissues [2]. Cutting force and chip formation are crucial indices of machining performances. Comparing the chip formation of orthogonal cutting of a regular ductile and brittle

material, as can be seen in Figure 1-2, shows the possibility of different cutting mechanics between ductile and brittle materials. The chip could be formed in several different ways for different material properties which could be explained by the dominant mechanism of cutting. It will be discussed in the next section.

The workpiece material properties, therefore, could range widely from brittle to ductile and from isotropic to anisotropic. To deal with a complex cutting configuration, numerical simulation is often adopted owing to the advancement of computational power and software development. Simulation models also enable more comprehensive analyses on cutting forces and chip formation, which are important parameters of machining performance [3].

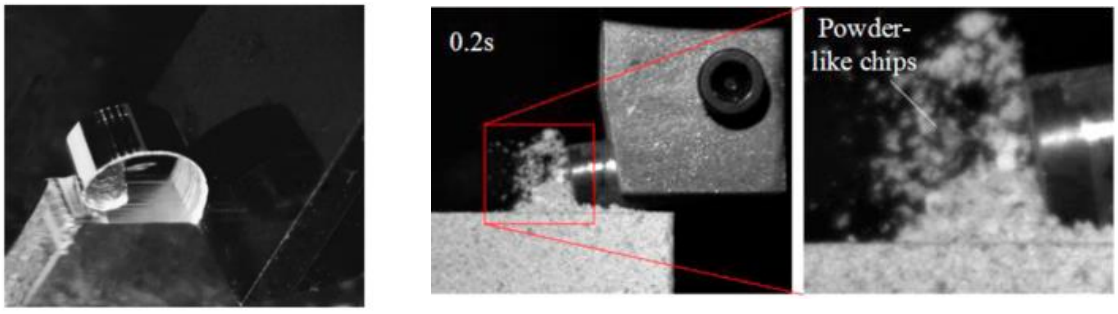

(a) (b)

Figure 1-2. Chip formation of orthogonal cutting of regular (a) ductile [4] and (b) brittle [5] materials

1.2. Motivation

Although brittle materials machining is a common process in industry, it is still very challenging for manufacturers, mainly due to lack of knowledge in brittle cutting

mechanics. So, the main motivation for this study was to address such industrial need through a fundamental study. The current research focuses on the mechanics of brittle materials cutting by understanding the dominant cutting mechanism. The cutting behavior including the chip morphology and cutting force was also investigated.

Even though machining of brittle materials has been widely used in manufacturing, there is no comprehensive and robust method to model brittle materials cutting. In order to address this issue, this study investigates the modeling of brittle materials cutting such that the model can predict the chip morphology as well as cutting forces.

Several researchers have attempted to model the cutting of brittle materials such as bones, ceramics, and carbon-fiber reinforced plastics (CFRP). The analytical approaches for brittle cutting such as bone cutting are very limited due to the complexity of the nature of the problem [6]. So, the main focus then has been attracted towards the numerical modeling. The literature review on the modeling of different brittle materials cutting will be presented in the next chapter.

1.3. Objectives

Machining of brittle materials has been widely used in the manufacturing world, while it is still one of the most difficult and challenging works for manufacturers, mainly due to lack of knowledge in brittle cutting mechanics. Several research groups have been trying to develop computational models for crucial brittle materials cutting processes such as the cutting of bone, ceramics, fiber carbide and so forth. However, there is not a generalized computational method yet that is capable of predicting chip formation as well

as cutting forces precisely. Even among those models which are not completely efficient and applicable, there are some discrepancies, not only in model setup, but also in definition of the failure criteria [3].

As explained in the last section, the difficulty of cutting of brittle materials over ductile materials can be associated to the role of fracture and crack propagation. The chip formation of ductile material cutting is usually continuous and curled, but the brittle cutting mostly generates powder-like chips, chunk-like chips, fragmented debris, or series of discrete chips, all due to fracture. The existing computational models for cutting like regular FEM is not able to capture crack propagation. Even some modified FE methods, such as cohesive zone-based FEM requires pre-defined crack paths which limits this model for very simple geometries; the cases that we already know where the crack is going to initiate and propagate. The other approach could be using particle-based computational models such as SPH, instead of element-based models like FEM. However, this is a very novel method for cutting and needs a deep understanding of the physics behind the model to be able to apply that correctly.

1.4. Organization of the Dissertation

The dissertation follows the common format of a journal paper such that it includes a complete and distinct research topic, yet under the umbrella of the main dissertation title. Each chapter includes a short summary, an introduction, the main research including materials & methods, and results & discussion and the conclusion.

Chapter 2 reviews the methods to model bone, ceramics and composites cutting. A comprehensive review on bone cutting is presented in this section since the chosen materials to do the experimental tests and numerical modeling is a bone-mimic material.

As mentioned above, machining of brittle materials is common in the industry, but there is no robust model to predict the cutting behavior. Smoothed particle hydrodynamics (SPH), which is a particle-based method, recently began to appear in the modeling of orthogonal cutting but has not yet been validated by experimental data. Then, the feasibility of SPH in brittle cutting simulations is thoroughly investigated in Chapter 3. The model setup including how to create the SPH domain and tie it to the FE domain is discussed. Then, the effects of particle density and damage criteria are studied.

The limitations of SPH method might hinder its application for brittle cutting modeling and requires further study and model development. Thus, a novel fracture-based finite element method is proposed in Chapter 4. To develop this method, the cohesive zone concept is used. The implementation of the method including how to embed a network of CZ elements and input the material properties are discussed. To build a successful model, a scaling factor is introduced and different scenarios are studied to thoroughly understand the effects of this factor.

By ensuring a complete model by ECZ-FEM, the experiments for validation study are performed in Chapter 5. The chip formation and cutting forces predicted by the ECZ-FEM model are compared against experiment.

Finally, the research conclusion is drawn and the room for future work and improvement is discussed in Chapter 6.

2. LITERATURE REVIEW*

This chapter reviews the literatures on bone, ceramics and composites cutting modeling. Because the brittle material selected for both simulation and experiment in this study is a bone-mimetic material, a comprehensive literature review of the numerical modeling of bone cutting[1] is presented in the following section.

2.1. Computational Methods

As mentioned in the last chapter, the modeling of brittle materials cutting can be in the forms of analytical approaches or computational methods. That said, analytical methods do not seem to be practical to such complex engineering problems which involve the interaction between the cutter and the workpiece. So, researchers have focused to develop computational models for this purpose.

2.1.1. Bone cutting modeling

Bone cutting is a critical process in surgical operations. Cutting of bone, which tends to be a brittle material, needs to be carefully operated to assure a precise surgery with the minimum damage to the human body.

There are a large number of FEA studies focused on bone orthogonal cutting. Orthogonal cutting is a 3D process per se [7]; however, except few works considering

[1] Content of this section has been adopted with permission form: B. Takabi, B.L. Tai, "A review of cutting mechanics and modeling techniques for biological materials," *Medical Engineering and Physics*, 45 (2017) 1-14.

three-dimensional orthogonal cutting [8, 9], the majority of studies [10-17] on metal and composite orthogonal cutting have seen this process as two dimension to reduce computational cost. In addition, there are also a couple of recent models using a mesh-free method, which will be introduced.

2.1.1.1. FEM: Johnson-Cook (J-C) based models

Alam et al. [18] performed a 2D simulation on bone orthogonal cutting using the commercial software MSc Marc. The schematic of the geometry and boundary conditions considered for the FEA model is shown in Figure 2-1. They assumed an elastic-viscoplastic as well as isotropic behavior for the cortical bone. Cutter geometry, depth of cut, and cutting speed were variables in the model to test the cutting performance. In addition, a shear friction model was used as opposed to the conventional Coulomb's friction. The coefficient of friction was 0.35 by using the similarity to bone-wood interaction.

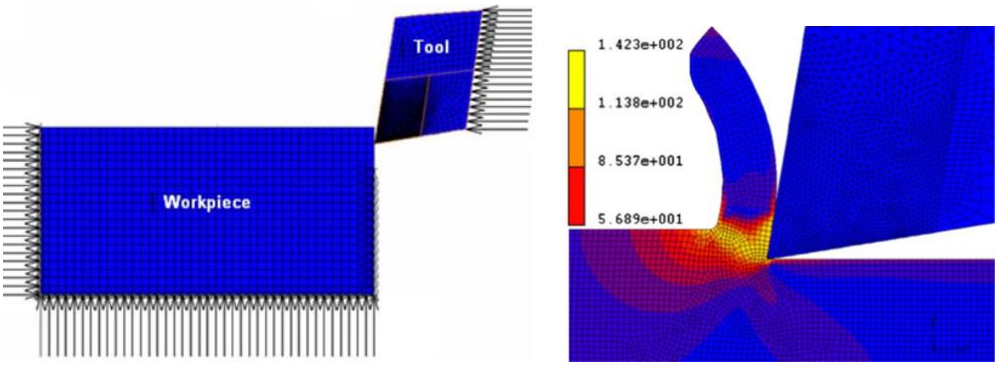

(a) (b)

Figure 2-1. (a) The schematic of the geometry, mesh and boundary conditions, (b) equivalent (von Mises); reprinted with permission from [6]

Johnson–Cook (JC) model was employed for the non-elastic behavior of the bone during cutting. This model has been widely used for metal cutting [11, 19-24] because it takes into account strain hardening, strain rate sensitivity and thermal softening which are presented in the first, second and third terms, respectively, of Eq. (2-1).

$$\bar{\sigma}(\bar{\varepsilon}^p, \dot{\bar{\varepsilon}}^p, T) = [A + B(\bar{\varepsilon}^p)^n]\left[1 + C\ ln\left(\frac{\dot{\bar{\varepsilon}}^p}{\dot{\bar{\varepsilon}}_0}\right)\right][1 - (\frac{T - T_0}{T_m - T_0})^m] \quad (2\text{-}1)$$

where $\bar{\varepsilon}^p$ represents strain hardening, $\dot{\bar{\varepsilon}}^p$ stands for the strain rate sensitivity. Also, A, B and C, are constants; n and m are the exponents for the strain hardening; temperature sensitivity. T_0 and T_m are the initial and the melting temperatures, respectively. Alam et al. neglected the temperature term in J-C model because of little temperature softening effect. Other constants in J-C model were determined based on curve fitting on the stress-strain curve resulted from the tension test [18]. They assessed the effects of the depth of cut, friction coefficient, and nose radius of the cutting tool on the forces. These effects were validated by experiments using the mid-diaphysis of a fresh bovine femur. Along the same line, their research group extended the approach to account for temperature effects [25], where the thermal properties were directly adapted from those reported by Davidson and James [26] and Huiskes [27]. However, no damage criterion was specified in these works, so a continuous chip was expected as can be seen in Figure 11(b). Alam et al. [28] also applied the same concept to ultrasonically-assisted cutting of bone to investigate cutting forces and thermal impacts.

Childs and Arola [29] investigated the applicability of using metal machining models to simulate cortical bone cutting, with bone being isotropic and elastic-plastic. The cutting

tool was a conventional shaper with triangular tool inserts. Their material properties were obtained from another paper [30]. The simulation was performed utilizing a commercial metal cutting software AdvantEdge-2D^{TM}. The material model was based on isotropic elastic-plastic behavior plus a damage criterion. The yield stress was pressure dependent based on Drucker-Prager yield criterion [31]. The isotropic hardening behavior describes the stress flow by a power law form of strain rate and strain, as well as the thermal softening effect, as shown in Eq. (2-2).

$$\bar{\sigma}(\bar{\varepsilon}^p, \dot{\bar{\varepsilon}}^p, T) = \sigma_0 \left[1 + \frac{\bar{\varepsilon}^p}{\bar{\varepsilon}_0^p}\right]^{1/n} [1 + \dot{\bar{\varepsilon}}^p]^{1/m}\, \Theta(T) \tag{2-2}$$

The $\Theta(T)$ represents thermal softening, which was neglected here due to small increase of temperature during bone cutting, similar to the assumption made by Alam et al. [18]. The parameters σ_0, $\bar{\varepsilon}_0^p$, n, and m were obtained from the literature [30]. A progressive damage was applied where an element lost its stiffness when the damage fraction D reached 1.0, such that

$$D = \sum \frac{\Delta\varepsilon^p}{\varepsilon^f} \tag{2-3}$$

where $\Delta\varepsilon^p$ was the increment of the equivalent plastic strain, and ε^f was the equivalent strain at failure. The ε^f was based on the Johnson-Cook failure model, but not specified in this work.

They also studied the effects of different parameters involving in an orthogonal bone cutting for ductile to brittle behaviors (referred to "ductility ranking"). The ductility ranking was adjusted by altering parameters for ε^f. The specific cutting force, a normalized

cutting force by the uncut chip area, was shown to be influenced by Young's modulus, Poisson's ratio, cutting edge radius, and depth of cut, and the ductility ranking. Among them, the ductility ranking has the most dominant effect. In addition, they also investigated the effects of the friction factor for a range of ductility ranking by using two values of the friction factor 0.2 and 1. The value of 0.2 was obtained from experimental works, while μ = 1 indicates an extreme condition when friction stress becomes limited by shear flow stress. As the results shown in Figure 2-2, the chip formation and force are highly dependent on these parameters.

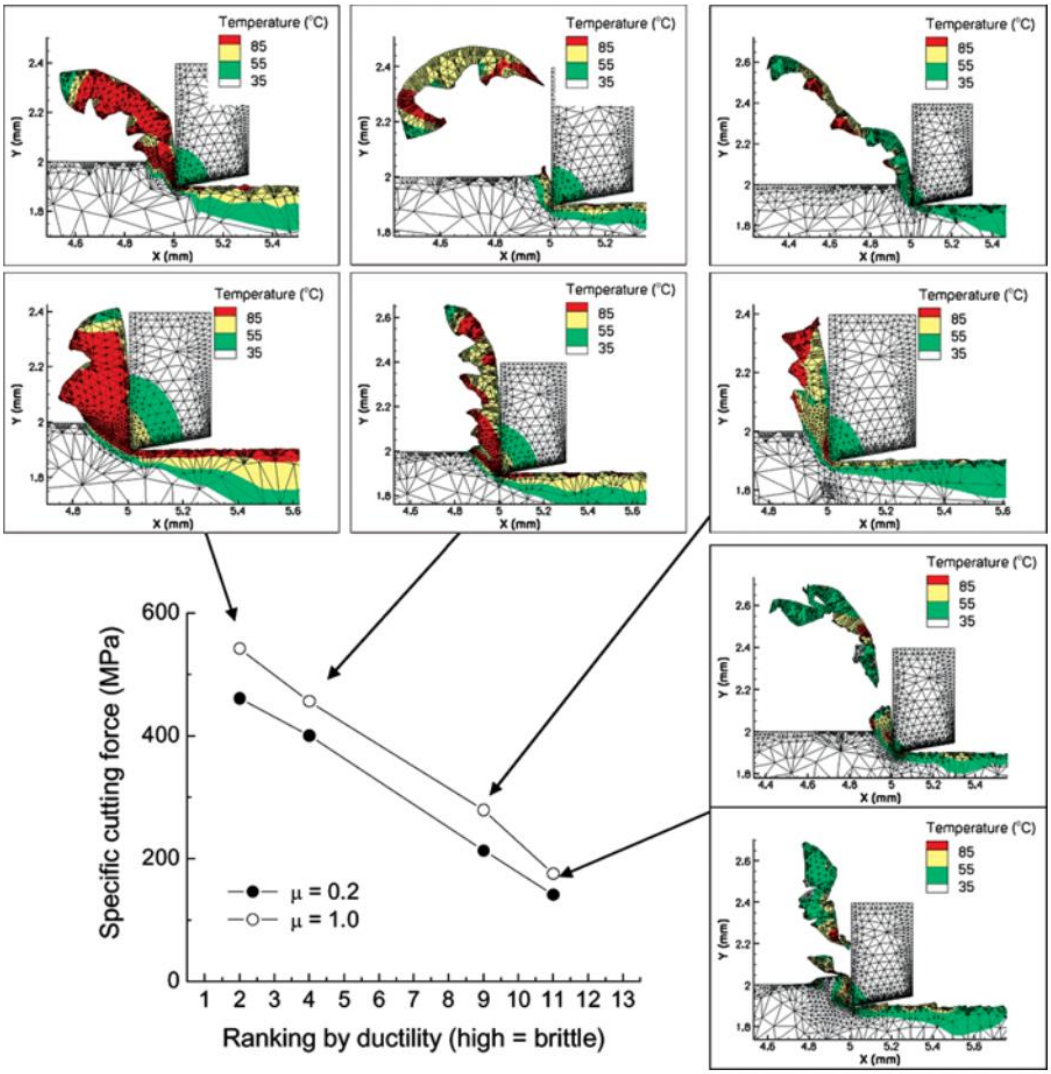

Figure 2-2. The specific cutting forces and chip formation, (in each pair of images, μ=0.2 is above and μ=1 is below) [29]; reprinted with permission from [6]

More recent papers incorporated the effects of anisotropic behavior of bone on the cutting characteristics. Santiuste et al. [32] included anisotropy effect to the diaphysis of long bones through a VUMAT user subroutine in Abaqus. They made both two and three-dimensional models for their simulations, and also considered both isotropic (2D) and anisotropic behavior for the bone (3D). For the isotropic model, the J-C model was used

with the temperature term neglected. Likewise, the material properties and J-C model parameters were from [18]. The friction factor of 0.35 was taken from [25]. For the anisotropic behavior modeling of bone, they assumed an elastic behavior up to failure according to Hou's model [33], which is based on the composite mechanics of fiber-reinforced matrix. Hou's damage criteria were modeled via a VUMAT that follows a certain procedure to degrade material properties.

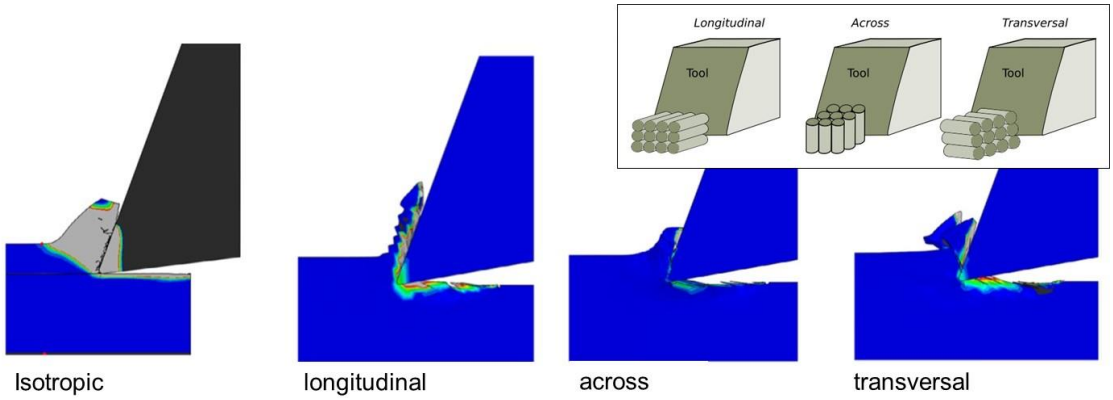

Figure 2-3. chip formation obtained from isotropic model, as well as anisotropic models including longitudinal, across, and transversal orientations [32]); reprinted with permission from [6]

Figure 2-3 shows their numerical results for the isotropic model and the anisotropic model in three osteon orientations (i.e., longitudinal, across, and transversal). This figure shows different chip formations. The average cutting force for the across orientation is higher than that of longitudinal orientation; the transversal orientation results in the highest force among these four models.

Although cortical bone is well known as being anisotropic, very few studies have used composite mechanics to simulate bone cutting [32]. This could be due to the fact that

modeling anisotropy of bone is much more complicated and time-consuming than isotropic cases.

2.1.1.2. Mesh-free models

Although FEA is widely used in cutting simulation, FEA models often face the issues associated with excessive element distortions and/or penetration. An adaptive remeshing method, associated with the remapping technique, might be used to mitigate these issues. However, it could be time-consuming and requires very fine mesh to generate accurate results. Alternatively, researchers have recently explored the feasibility of using the smoothed particle hydrodynamics (SPH) method to simulate cutting processes [34-39]. SPH is a meshless Lagrangian method and has been widely used in fluid dynamics analyses. In this technique, material properties are approximated by their values on a set of discrete points, or called SPH particles. This way avoids mesh tangling and distortion problems in FE large deformation simulations [34].

Li et al. [40] used a hybrid FEA-SPH model to simulate bone cutting with a steel blade. The bone material was the mid diaphysis of a fresh bovine femur. The area of the workpiece under the cutter is modeled by SPH for contact and cutting simulation, while the rest of the workpiece is modeled by FEA, as shown in Figure 2-4(a). They took the anisotropic behavior of bone into account. For the SPH domain, the smoothing length was 2.2 times of the characteristic length of the associated particle volume. Also, particle elements (PC3D in Abaqus) have been used for the SPH domain, and the coefficient of friction was set to 0.3 in accordance with [41]. The bone mechanical behaviors were

modeled as a transversely isotropic, elastic-plastic material along with Hill's anisotropic yield criteria and progressive damage. The Hills' yield criteria can be described by

$$F(\sigma_{22}-\sigma_{33})^2+G(\sigma_{33}-\sigma_{11})^2+H(\sigma_{11}-\sigma_{22})^2+2L\sigma_{23}^2+2M\sigma_{31}^2+2N\sigma_{12}^2=1 \quad (12)$$

where *F*, *G*, *H*, *L*, *M*, and *N* are constant determined from another literature. The material properties were obtained from the previous experimental data by the same research group. The onset of damage was assumed at a failure strain of 0.02 [42]. The damage evolution was governed by the energy-based criterion to describe the progressive degradation. This value was not specified in the paper.

Their results revealed that considering progressive damage along with the anisotropic property significantly affects the material response to the cutting blade, especially for cortical bone which is a quasi-brittle material. Figure 2-4(b) shows the simulated crack propagation during cutting when the osteons are oriented in different ways. Accordingly, they suggested that damage criteria must be taken into account for the large deformation simulations. Otherwise, it might lead to inaccurate results such as an unrealistic continuous growth of cutting force.

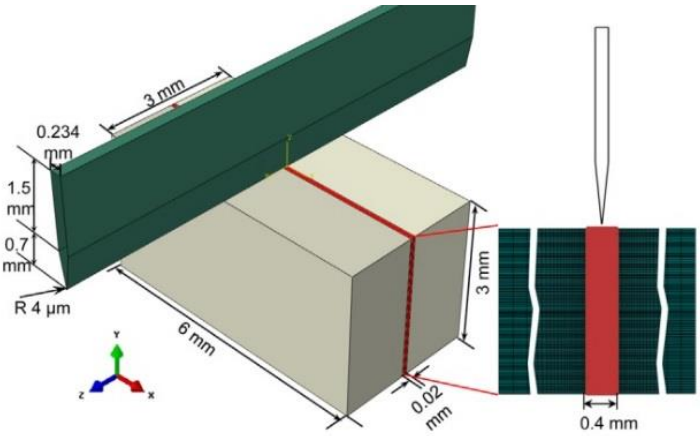

(a)

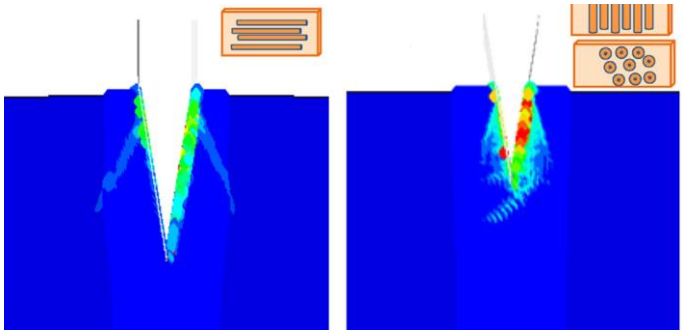

(b)

Figure 2-4. FEA-SPH bone cutting simulation (a) Geometry of the cutting tool and workpiece, and FE and SPH domains, (b) The crack propagation of different orientations of osteons [40]; reprinted with permission from [6]

Similarly, Tajdari and Tai [43] also introduced an FEA-SPH hybrid model for 3D bone drilling, particularly for Kirschner wires (K-wires) made of stainless steel. Unlike regular drill bits, a typical K-wire has a trocar tip and does not cut continuous chips. Thus, FEA cannot capture the small bone debris generation. In their work, the SPH domain (element PC3D in Abaqus) was placed in the workpiece under the drill tip for a full cutting edge contact, as shown in Figure 2-5(a), while the rest of the workpiece was made as FEA domain (element C3D8R). The grid size was set 0.05 mm, smaller than the feed per

revolution of the tool 0.07 mm. For both SPH and FEA counterpart, an isotropic, elastic-plastic material property was used. The friction factor was assumed to be 0.2. The damage of element was initiated at 0.033 strain followed by an immediate failure to simulate an extremely brittle scenario. For this purpose, the effective plastic displacement was assumed with 1 μm displacement. Figure 2-5(b) illustrates the results of K-wire bone drilling with SPH (left) and FEA (right). As shown, SPH produced a large amount of tiny bone debris from the model and accumulated on the workpiece surface. These debris fragments, though failed in the model, still interact with the tool and workpiece. On the contrary, FEA simply deleted the failed elements. Therefore, the force and torque profiles of SPH were higher and more continuous than FEA, although they were not yet experimentally validated in the paper.

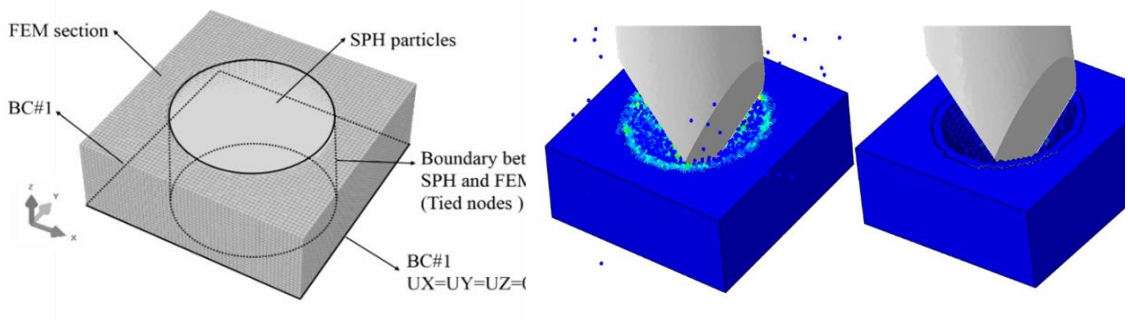

(a) (b)

Figure 2-5. FEA-SPH simulation of K-wire bone drilling (a) Geometry, as well as the SPH and FE domain (b) Chip formation by SPH (left) and FEA (right) [43]; reprinted with permission from [6]

In summary, Finite element method (FEM) has been applied in bone cutting research to study forces, damage, and heat generation. Many articles have adopted the

Johnson-Cook (J-C) plastic model to simulate the material deformation. Some papers do not specifically take damage definition into account, while others suggest that the damage criteria must be defined [6]. The differences in the model setting can affect both chip formation and cutting force results significantly. In addition to FEM, some recent papers adopted particle-based models for bone cutting and brittle materials cutting, such as smoothed particle hydrodynamics (SPH), but they have not been fully validated experimentally [3].

2.1.2. Modeling of ceramics and composites

For ceramics cutting, the chip formation is in a shape of a series of discrete chips due to brittle fracture [44]. In the regular FEM, the elements are removed after failing, *i.e.*, exceeding the damage criteria; therefore, it cannot predict the crack propagation. Thus, for modeling brittle materials, the path of crack propagation must be pre-defined. Typically, a small crack or notch is placed in the domain so that it makes the tool move along with the crack path to keep its contact with the workpiece [45]. Cohesive zone FEM (CZ-FEM) has been frequently used to model such brittle behaviors [46-48]. The details of this method will be discussed in the next chapters.

The other brittle material which is widely used in aerospace industries and needs to undergo cutting processes is carbon-fiber reinforced plastics (CFRP). It has been observed that, during cutting of this material, micromechanical damage, delamination and fiber pullout are highly dependent on the orientation of the fibers. So, regular computational schemes such as regular FEM have been unsuccessful in predicting this

effect. Similar to ceramics cutting, in order to model CFRP cutting processes, CZ-FEM has been used in the literature [49-51]. However, this method again requires predefined crack paths.

2.2. Conclusion

To model brittle materials cutting, analytical approach does not seem to be applicable due to the complex nature of the problem. Therefore, researchers have tried to develop a numerical model which can describe cutting behavior including the chip morphology as well as the cutting force.

To model bone cutting, the literature review reveals that to model bone cutting, FEM has been used along with the Johnson-Cook (J-C) plastic model to describe material behavior. However, there are some discrepancy in the literatures, such as damage criteria which governs the element degradation and deletion. These discrepancies have affected the numerical results like chip formation and cutting force. Further study, especially on the damage criteria, is needed to build a comprehensive model which can predict both chip formation and cutting force of bone cutting. The review demonstrates that an appropriate damage criterion should be into account, while some papers have not considered that. Another method to model bone cutting is meshfree methods such as SPH. However, it has not experimentally validated and needs further study.

In ceramics and composites cutting processes, the dominant mechanism of cutting is fracture which leads to crack initiation and propagation. The regular FEM, then, cannot be used for such modeling because it cannot capture the crack, unless an extremely fine

mesh is used which is not practical for engineering applications. The researches have used the cohesive zone FEM (CZ-FEM) to model such brittle materials behavior. The CZ elements are placed at the interface of two materials, or for composite cutting, they are placed along with the fibers, where the crack is anticipated to occur. So, CZ-FEM requires predefined crack path. But for orthogonal cutting of brittle materials, this method cannot be used because of undetermined fracture and crack. Therefore, there is a need to develop a method to model the orthogonal cutting of brittle materials which does not require predefined crack path.

3. FEASIBILITY OF SPH IN ORTHOGONAL CUTTING SIMULATIONS*

Synopsis

This chapter[2] conducts a numerical study of smoothed particle hydrodynamics (SPH), a mesh-free method, for orthogonal cutting simulations of both ductile and brittle materials. Finite element method (FEM) is commonly used for cutting simulations, but issues with excessive element deformation hinder its applications. SPH can be an alternative option because of the particle-based algorithm eliminating the use of volumetric elements. However, studies have reported inconsistent ways to set up damage definition and particle density. This chapter instructs a method to build an SPH model and compares the results with an equivalent FEM, in terms of the effects of damage definition and particle density on chip morphology and cutting forces. The materials used for this study are aluminum, which represents a common ductile engineering material, and the cortical bone representing a brittle counterpart. The results reveal that in spite of the natural separation of SPH, proper damage criteria must be defined for the model accuracy. SPH tends to produce a lower cutting force than that of FEM. SPH and FEM have an opposite convergence trend as the particle density/mesh size reduces. SPH better simulates fragmented debris in brittle cuttings but fails to produce curled chips in ductile cuttings. In order to resolve the limitations of this method which mostly comes from lack of control

[2] Content of this chapter has been adopted with permission form: B. Takabi, M. Tajdari, B.L. Tai, "Numerical study of smoothed particle hydrodynamics method in orthogonal cutting simulations–Effects of damage criteria and particle density," *Journal of Manufacturing Processes*, 30 (2017) 523-531.

on the natural separation of particles, further study is required. So, there might be a need to develop a different method for modeling of brittle materials cutting.

3.1. Introduction

Orthogonal cutting is the basic configuration of all machining processes to describe the interaction between the cutting tool and work-material. This cutting concept has been applied to a variety of fields from traditional metal alloys, brittle ceramics, to non-engineering materials such as rocks and human tissues [52-55]. The work-material properties, therefore, could range widely from brittle to ductile and from isotropic to anisotropic. To deal with a complex cutting configuration, numerical simulation is often adopted owing to the advancement of computational power and software development. Simulation models enable more comprehensive analyses on cutting forces, chip formation, and heat generation, which are important indices of machining performance.

The most common numerical tool for machining analyses is finite element method (FEM). FEM has been employed to simulate the cutting processes of metals [56], composites [50], and biological objects [57], among which metal cutting is considered the most well-developed application since the 90s [13, 58, 59]. Model setups such as mesh size, element type, and element damage model are known to significantly affect the simulation results. Since material separation is achieved by removing damaged elements, it becomes challenging when excessive deformation and stress concentration occur at the cutter-material contact. This challenge later led to the use of Arbitrary Lagrangian-Eulerian (ALE) method and re-meshing techniques which handle stress concentration and

avoid numerical issues during the computation. Similarly, commercial software Third Wave Systems [60] uses adaptive meshing techniques to re-mesh the cutting zone near the tool tip [61] at each time increment. However, these advanced techniques are often at a high computational cost [62, 63]. In order to tackle such issues with FEM, Smoothed Particle Hydrodynamics (SPH) began to appear in the field of manufacturing.

SPH is a mesh-free method that was first employed for astrophysics application and then has been gradually extended to the continuum mechanics scale [38]. SPH has been extensively used to obtain an approximate solution of fluid dynamics by replacing the flow domain with a set of particles [64]. SPH does not require the gridded domain like FEM. Thus, it can deal with problems involving free surfaces, deformable boundaries, moving interfaces. As a result, it can handle extreme deformation and even crack propagation [65]. SPH seems to be an alternative to FEM for machining processes [66, 67].

A few articles have investigated the feasibility of SPH for metal cutting simulations because it eliminates the issues associated with element distortion. Limido et al. [38] simulated the orthogonal cutting with a two-dimensional (2D) SPH for aluminum to obtain the cutting forces and chip formation. They used the Johnson-Cook model to define the material's plastic behavior, but the natural separation of particles to simulate material removal. They reported a 30% difference between the simulated cutting forces and experimental data. Calamaz et al. [63] analyzed the tool wear of Ti6Al4V via a 2D plain strain SPH using the J-C material constitutive model without damage definition. They mentioned that an insufficient particle density led to an error of 20% in shear band thickness. More recently, Julean [37] performed a 3D SPH orthogonal cutting simulation

of the aluminum alloy 6060-T6. Unlike the aforementioned articles, they defined damage in addition to the J-C constitutive model. The damage definition was based on Cockcrof-Lathram (CL) criterion. An underestimated error of 27% was reported compared to the experimental cutting force. Spreng and Eberhard [68] investigated the metal orthogonal cutting processes via both 2D and 3D SPH simulations for engineering steel C45E by implementing a cumulative-damage fracture model. In a similar work, Umer et al. [69] showed that the standard SPH was unable to simulate curled chips although they had defined a strain-based damage criterion. A modified SPH called Renormalized SPH can be used to correct the numerical issues.

The literature review of SPH orthogonal cutting simulations shows inconsistencies in the SPH modeling setup. In particular, some researchers use damage definition to model material separation, while others adopt the natural separation of particles. Even among those defining damage, there has not been a clear method to model the post-failure region. A quite number of articles have emphasized on the significant influence of damage definition in cutting results [63, 70]. Besides, the effect of SPH particle density is not as well-understood as that in FEM cutting simulations. Furthermore, all these works use SPH cutting simulations for metallic materials, while the performance of SPH in brittle materials is still unknown.

To justify the use of SPH in different cutting scenarios and a proper material setting, this research investigates SPH orthogonal cutting simulations for ductile and brittle materials, using FEM as the baseline. In particular, this chapter instructs a method for acquiring SPH from FEM. Work materials are aluminum alloy, which is a typical ductile

metal [71, 72], and the cortical bone, which is of interest to many orthopedic drilling studies [73-75]. Cortical bone is relatively brittle [40] and challenging in simulation due to small debris. This study focuses on the effects of damage criterion definition and particle density. Numerically generated cutting force and chip morphology resulted from SPH are directly compared with those from a converged FEM. No experimental study is included since this work is not aimed at a specific application. On the other hand, experiments can induce other uncertain parameters, such as friction, geometrical accuracy, and material properties that require tuning of models. Thus, FEM serves as the controlled counterpart. It should also be mentioned that this study does not consider the micro structural based response of cutting.

To structure this work, Section 3.2 explains the model setups for both FEM and SPH. This section covers the material definitions, including the damage criteria. Section 3.3 presents the computational results by SPH and FEM and investigates the effects of aforementioned parameters. Following this part, Section 3.4 is the discussion about the pros and cons of SPH over FEM and their applicable scenarios. Conclusions will be drawn at the end of this chapter.

3.2. Numerical Models and Testing Methods

3.2.1. Model configuration

ABAQUS/EXPLICIT (Version 6.14-2) was adopted for the orthogonal cutting simulation as it has both FEM and SPH modules. Figure 3-1 shows the schematic of the

model setup. A three-dimensional orthogonal cutting was first created in FEM with the workpiece dimensions of 5.0 mm (height) × 10.0 mm (length) × 0.4 mm (width). The depth of cut (DOC) is 0.4 mm. Although the orthogonal cutting was often described in a 2D scenario, this simulation was performed in three dimensions to test the 3D capabilities of SPH. The model was built with three layers with the top one (chip layer) having a smaller mesh to handle material deformation and separation, as shown in Figure 3-1(a). The second layer was a transition to the bottom layer that has a rougher mesh. This setup allows more efficient computation as the bottom layer does not effectively involve in tool-workpiece interactions. To assure having a continuous material throughout these three layers, the "tie" function was used to pin the particles and nodes in all degrees of freedom, as shown in Figure 3-1(a). The mesh independency was assured for the bottom and transition layers for the SPH simulations and also the entire computational domain for FEM. The particle density of the chip layer was a variable for comparison in a later section. The boundary of the bottom layer was fixed in three translational directions (X, Y, and Z). Two sides of the bottom layer were fixed in the normal direction (Z) to mimic a plane-strain condition, while only one side of the chip layer was fixed in the normal direction to emulate a thin chip in real cutting processes. With this FEM model, an equivalent SPH model can be built by converting the FEM nodes of each element (C3D8R) to SPH particles (PC3D). It should be noted that SPH does not have physical elements; the FEM nodes are directly converted to SPH particles. The particle spacing (L) is the same as the FEM element size, as shown in Figure 3-1(b). This spacing, which is twice of the "characteristic length" defined in ABAQUS, is used to calculate the volume of each

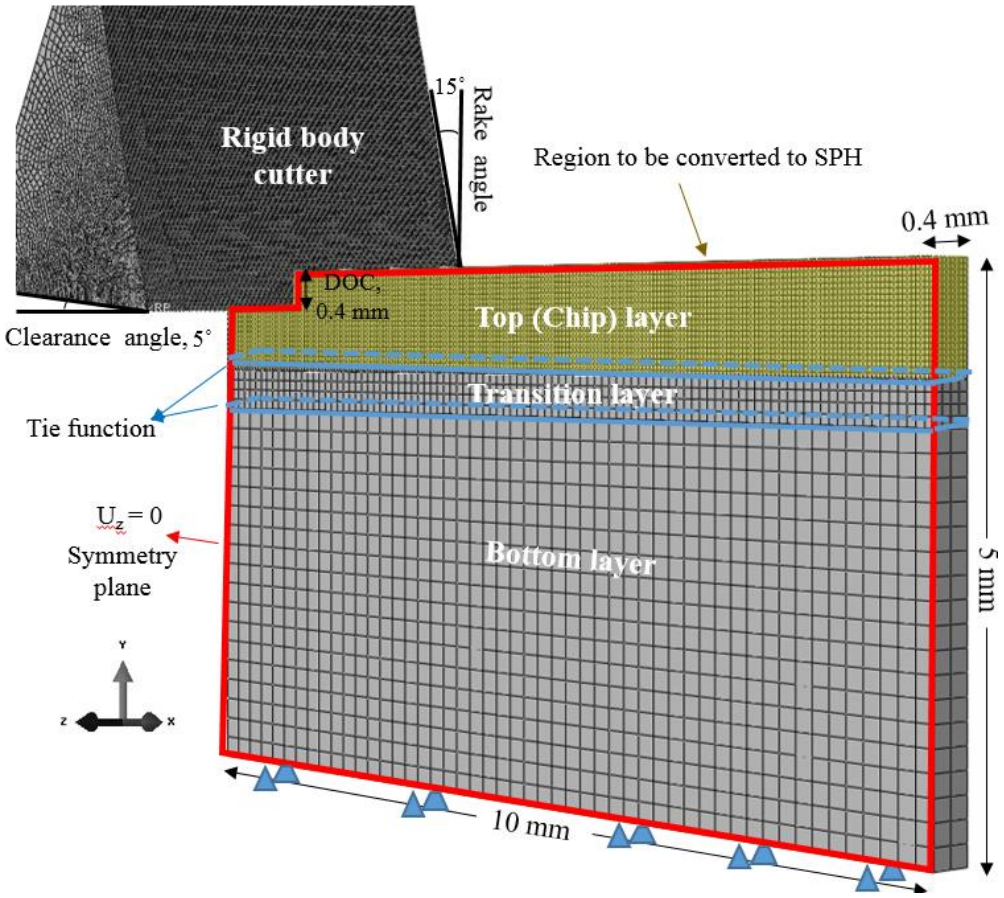

(a)

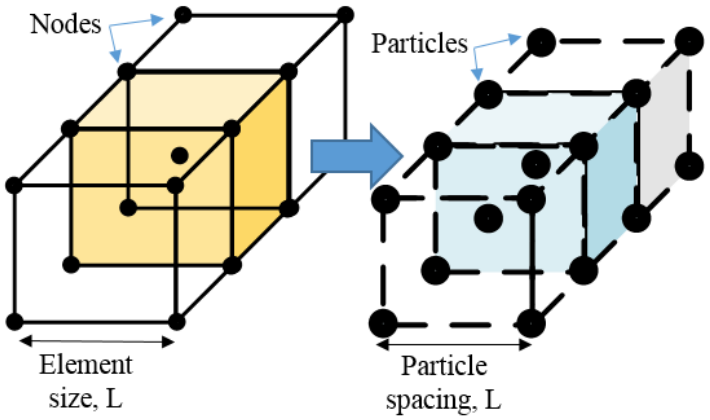

(b)

Figure 3-1. The schematics of (a) the model configuration and boundary conditions and (b) the conversion of FEM to SPH models; reprinted with permission from [3]

particle. Usually, SPH modeling is suggested to have evenly distributed particles, so a constant *L* can be used for the entire model [76]. For this reason, all the FEM elements were made cubic to ensure the compatibility during the FEM-SPH conversion.

Different from FEM, SPH approximates the field value based on the interpolation across the neighboring points weighted by a kernel function (*W*). A cubic spline form, as indicated in the equation below, was used for the kernel function [77-79].

$$W(r,h) = \frac{C_n}{h^n}\begin{cases} 1 - {}^3\!/_2\, x^2 + {}^3\!/_4\, x^3 & 0 \le x \le 1 \\ {}^1\!/_4\,(2-x)^3 & 1 \le x \le 2 \\ 0 & x \ge 2 \end{cases} \tag{3-1}$$

where $x = \frac{r}{h}$ is a dimensionless location of the particles; r and h represent the distance between the particles and the smoothing length, respectively. The normalization factor C_n assumes the following values depending on the problem dimension.

$$C_n = \begin{cases} \frac{2}{3} & n = 1 \\ \frac{10}{7\pi} & n = 2 \\ \frac{1}{\pi} & n = 3 \end{cases} \tag{3-2}$$

The smoothing length determines the number of neighboring particles. This length is automatically calculated in ABAQUS to include 30 to 50 particles by default. Stresses are then computed in a similar fashion as for reduced-integration brick elements, which are in turn used to compute element nodal forces, stress, strain and so on [79].

To ensure the uncut layers to have the same stiffness to support the cutting layer (the top layer) in SPH simulations, a hybrid model consisting of both SPH and FEM domains was generated rather than an entire SPH domain. Since SPH particles are

converted from the elemental nodes, the nodal positions remain the same, and thus the nodes on the interface between SPH and FEM are aligned with each other.

For machining and cutting tool setups, the cutting blade was modeled as a rigid part with a clearance angle of 5 degrees and rake angle of 15 degrees, as shown in Figure 3-1(a). The friction coefficient between the cutting tool and workpiece was 0.2, estimated based on [80]. A velocity of 400 mm/s (24 m/min) was applied to the rigid body cutter along the X-direction.

3.2.2. Material properties and damage criteria

Two materials are included in comparison: aluminum representing ductile materials and cortical bone representing quasi-brittle materials [71]. The detailed property definitions including progressive damage criteria are presented in this section.

3.2.2.1. Cutting of ductile materials

As a typical ductile material, the aluminum alloy selected was 2024-T351, which is commonly used in the manufacturing processes. The material properties of Al 2024 include the density of 2700 kg/m^3, the elastic modulus of 73 GPa and the Poisson ratio of 0.33 [72]. Aluminum cutting has been studied extensively [36, 61, 81]. Almost all the simulation works adopt Johnson-Cook (J-C) material model to describe the cutting mechanism [82]. Eq. (3-3) is a generic expression of J-C model for an equivalent plastic flow stress as a function of strain, strain rate, and temperature. The parameters used in this study are specified in Table 3-1 [72].

$$\bar{\sigma} = \left(A + B\bar{\varepsilon}^{n}\right)\left[1 + C\ln(\frac{\dot{\bar{\varepsilon}}}{\dot{\bar{\varepsilon}}_0})\right]\left[1 - \left(\frac{T - T_{room}}{T_{melt} - T_{room}}\right)^{m}\right] \tag{3-3}$$

Table 3-1. Johnson-Cook parameter values for Al2024-T351 [72]; reprinted with permission from [3]

A (MPa)	B (MPa)	n	D1	D2	D3	D4	D5
352	440	0.42	0.13	0.13	-1.5	0.011	0

The effects of thermal softening and strain-rate hardening were not considered here for two reasons. One, the thermal effect involves heat transfer analysis, which creates another uncertain factor in SPH's thermal simulation. Second, the cutting speed (400 mm/s) is a control variable; thus, the effect of strain rate change does not exhibit here. Pairing with the J-C plastic model is the J-C failure model to define when the element damage occurs, as can be seen in Figure 3-2, the material behavior reaches a phase of strain softening which is called damage evolution. This phase starts at a damage initiation point (D = 0), following by a gradual reduction in the load carrying capacity of the material. The initiation of the damage occurs when the increment of the plastic strain has reached the damage initiation strain $\bar{\varepsilon}_{0i}$ calculated by Eq. (3-4) [72].

$$\bar{\varepsilon}_{0i} = \left[D_1 + D_2\exp(\mathrm{D}_3\frac{p}{q})\right]\left[1 + D_4\ln(\frac{\dot{\bar{\varepsilon}}}{\dot{\bar{\varepsilon}}_0})\right]\left[1 - D_5\left(\frac{T - T_{room}}{T_{melt} - T_{room}}\right)\right] \tag{3-4}$$

where D_1 to D_5 are material constants listed in Table 3-1 [72]. In the damage evolution region, the plastic equivalent stress $\bar{\sigma}$ in the material is calculated by

$$\bar{\sigma} = (1 - D)\,\tilde{\sigma} \tag{3-5}$$

where $\tilde{\sigma}$ is the undamaged stress and D ranges from 0 to 1 with 1 being a complete material failure. The damage evolution is defined using Hillerborg's fracture energy, which can alleviate mesh dependency by creating a stress-displacement response after damage initiation. This approach adopts a stress-displacement response rather than a stress-strain response [72]. The linear damage evolution, which can be defined based on energy dissipated during the damage process, was considered (Eq. 3-6) [71].

$$D = \frac{\bar{u}}{\bar{u}_f} \tag{3-6}$$

where $\bar{u}$ is the equivalent plastic displacement; $\bar{u}_f$ represents the equivalent plastic displacement at failure, calculated by

$$\bar{u}_f = \frac{2G_f}{\sigma_y} \tag{3-7}$$

The fracture energy G_f can be calculated based on the fracture toughness K_c by Eq. (3-8). The fracture toughness of Al 2024-T351 is 37 MPa.m$^{1/2}$ [72]. Even though G_f in cutting processes can be a mixed mode, it tends to be dominated by *Mode I* for a positive rack angle tool [71].

$$G_f = \left(\frac{1-\upsilon^2}{E}\right) K_c^2 \tag{3-8}$$

Many studies do not specify their definition of damage evolution [20, 83-87]; sometimes the value is adjusted by trial and error [36]. The actual value may be

experimentally defined based on conducting fracture toughness test or fitting the energy release rate after the onset of necking in a tensile test.

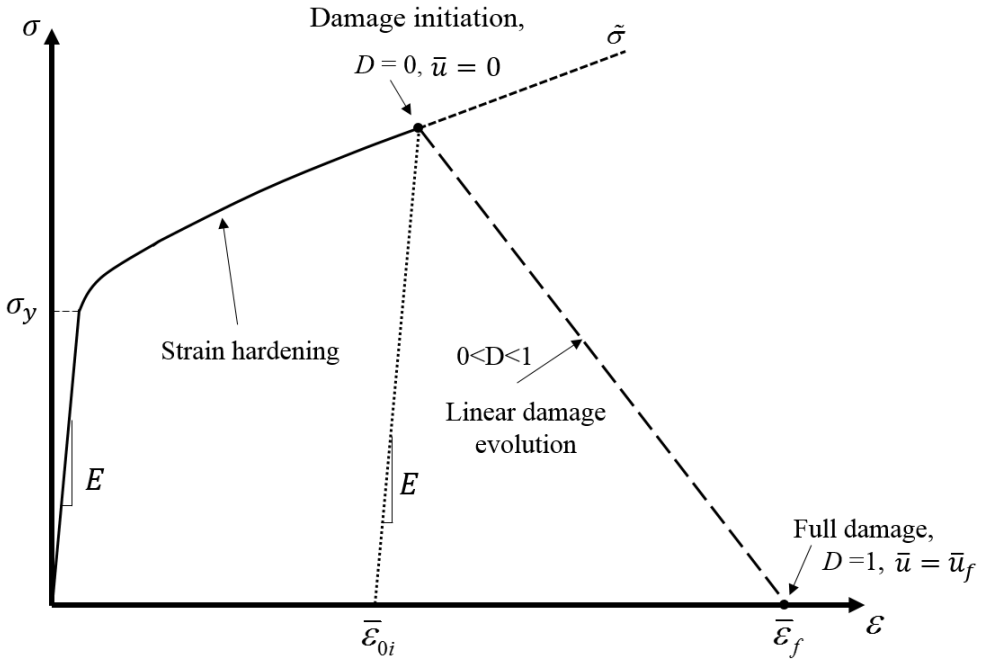

Figure 3-2. A stress-strain curve that describes the material behavior with damage definition; reprinted with permission from [3]

3.2.2.2. Cutting of brittle materials

The cortical bone which is generally considered brittle [88] or quasi-brittle [71] was chosen to cover the cutting of brittle materials in this study. Bone machining is of interest due to the concerns of thermal and mechanical injuries to living tissues. In this study, the cortical bone was considered isotropic since the numerical result was not compared to real bones. The density was set 2000 kg/m^3, the elasticity modulus was 10

GPa and Poisson's ratio was 0.4 [29]. The elastic-plastic model of the bone was adopted from [32] instead of using J-C model due to a very limited plastic region and the unknown J-C parameters. Similar to the aluminum model, damage evolution was calculated based on Hillerborg's fracture energy. The fracture toughness of this material is 5.45 $MPa.m^{1/2}$ [89].

3.3. Results

In this section, cutting force and chip morphology obtained from both SPH and FEM are presented for the two selected materials, Al 2024 and cortical bone. The SPH results are compared to an identical, converged FEM. This section also includes the effects of damage criterion and particle density for SPH on the simulation results.

3.3.1. Effects of damage criterion

Damage criteria are usually defined to allow material separation to simulate cutting. However, this definition is not necessary for SPH due to its "natural separation" of the particles under excessive stretch as mentioned in Introduction. To assess the effects of setting damage criterion, two cases were tested by SPH for each type of material with and without damage definition, called "damageable" and "undamageable" models hereafter. Only damageable FEM results are presented in this paper. As mentioned above, material damage is defined by two consecutive steps, damage initiation, and damage evolution. These two steps must be used in conjunction in order to execute the damage behavior correctly.

3.3.1.1. Simulation results of aluminum cutting

Fig. 3 illustrates the chip formation of aluminum cutting resulted from both SPH and FEM simulations. SPH with and without the damage definition are compared with the FEM baseline. A continuous and straight chip was formed in Figure 3-3(a) in the undamageable SPH model. Defining damage for SPH resulted in a similar chip formation, but at a lower stress level, as shown in Figure 3-3(b). Comparing the chip thickness between these two figures reveals that undamageable SPH generates a little thicker chip because more plastic deformation is allowed. This is because particles can move extensively and aggregate to increase the chip thickness. In comparison with SPH, Figure 3-3(c) shows that FEM allows element deletion and produces a curled chip similar to a real aluminum alloy cutting process [36, 72, 90].

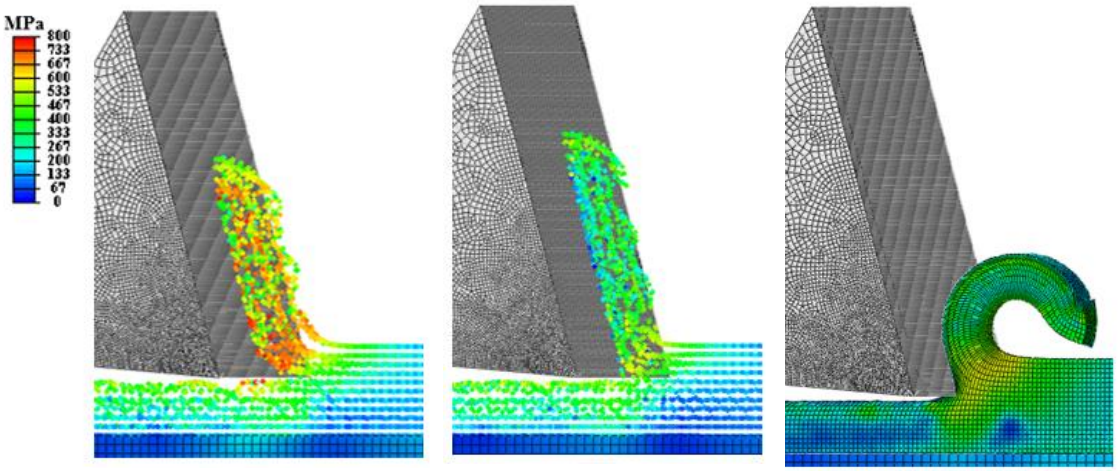

(a) (b) (c)

Figure 3-3. Effects of damage definition on the chip formation in the aluminum cutting simulation: (a) Undamageable SPH, (b) Damageable SPH, and (c) Damageable FEM; reprinted with permission from [3]

Figure 3-4 shows the results of the specific cutting force of the cases in Figure 3-3. Specific cutting force is defined as the cutting force per unit uncut chip area to normalize different cutting depths and feeds [29, 91]. Using the damageable FEM (Figure 3-3(c)) as the baseline, the force produced by undamageable SPH is closer to the baseline, but the force fluctuates significantly. The damageable SPH produces a smoother force profile, but the force level is about 20% lower than that of the baseline. These results show that the natural separation of particles in SPH can produce a reasonable cutting force. However, this observation does not necessarily lead to the conclusion that SPH requires no damage definition, which has been used in a few studies [34, 38, 92]. Theoretically, in FEM, a model without damage definition can infinitely increase the stress and strain level until the numerical error occurs. No damage definition prevents the elements from failure, leading to continuous deformation without a stop criterion [40]. However, in an undamageable SPH model, continuous deformation stretches the particles until they fall outside of the kernel effective region, leading to detachment from each other. Although SPH benefits from eliminating issues associated with excessive distortion, the phenomenon of natural separation is, after all, not a damage definition.

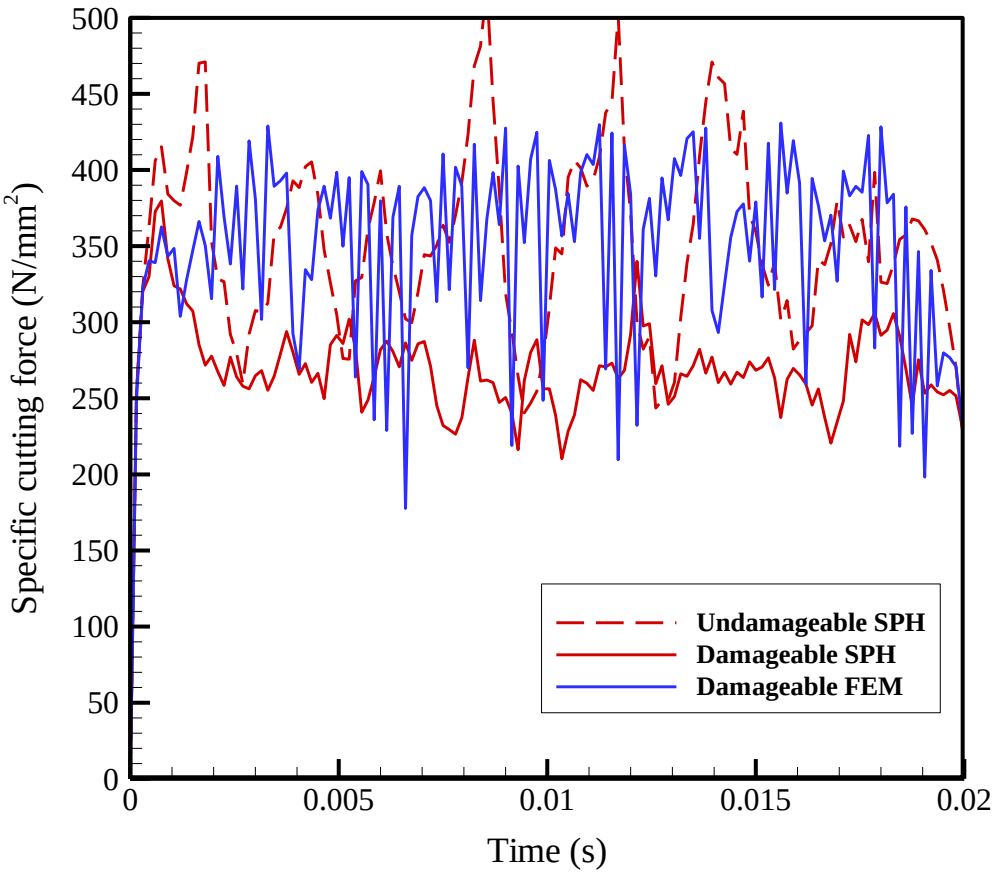

Figure 3-4. Effects of damage definition on the specific cutting force in the aluminum cutting simulation; reprinted with permission from [3]

Figure 3-5 illustrates the von Mises stress distribution along two designated paths. These two paths are shown in Figure 3-5(a) and (b) in the associated FEM and SPH simulations. Although the overall stress maps are similar, FEM shows higher stress values in *Path* 1 near the cutting edge compared to those of SPH, which explains the higher cutting force generated to the tool. On both paths, there is a smooth transition of stress from the transition layer to the chip layer; the stress values are small in the transition layer and nearly identical between SPH and FEM. These phenomena indicate that the tie

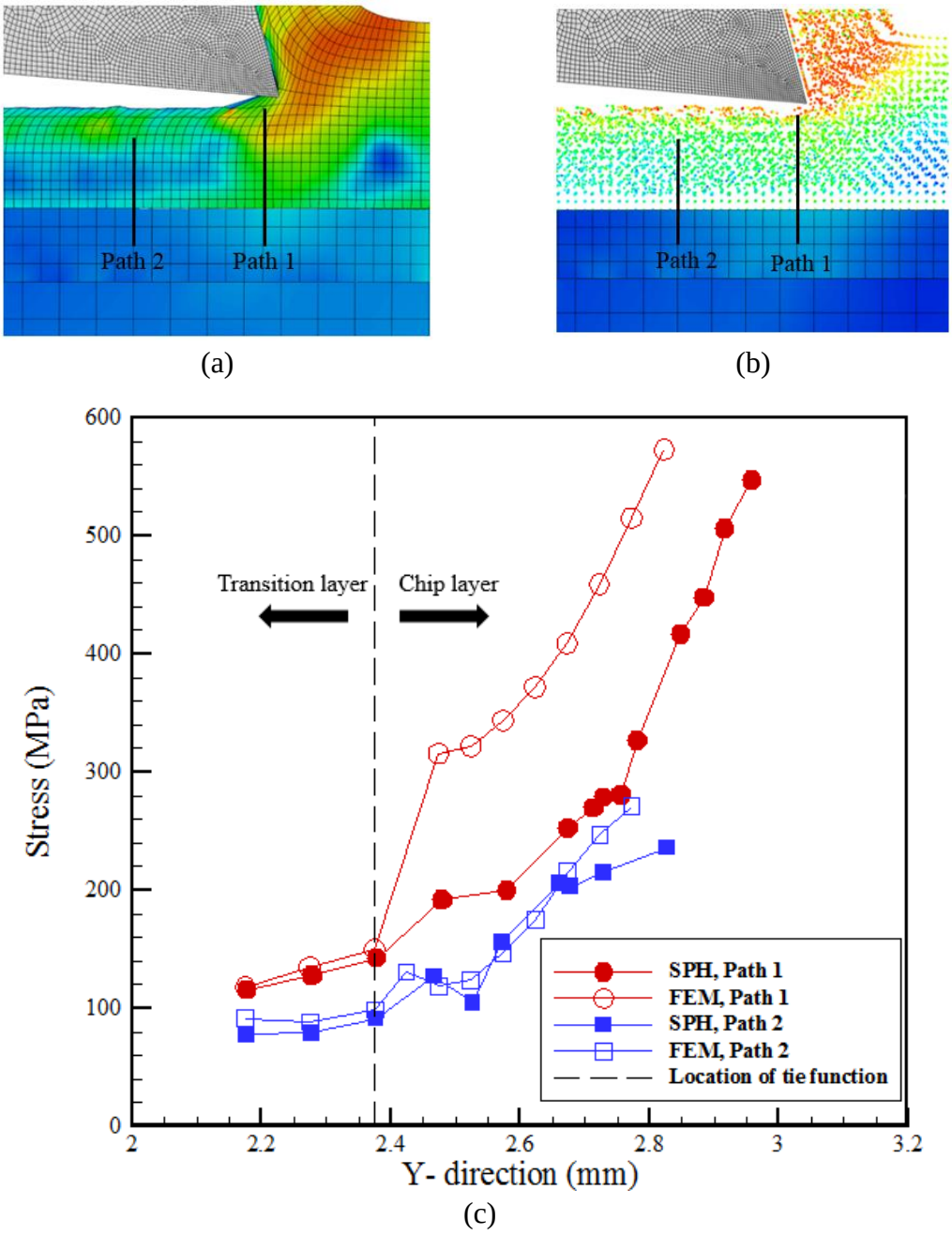

Figure 3-5. Stress variation along two designated paths, in the aluminum cutting simulation; reprinted with permission from [3]

function has been applied far enough from the high-stress region, thus not to affect the overall stress distribution.

3.3.1.2. Simulation results of bone cutting

Similarly, Figure 3-6 shows the chip morphology for SPH model with and without damage definition, as opposed to the corresponding damageable FEM. In Figure 3-6(a), a continuous chip was formed as a result of the natural particle separation, but this type of chip is unrealistic for a brittle material. Figure 3-6(b) shows the result of the damageable SPH, where the particles are separated apart from the surface. Since the equivalent plastic displacement at the failure ($\bar{u}_f$) for the cortical bone is less than half of $\bar{u}_f$ of the aluminum, particles lose their stiffness more rapidly and fail almost immediately after the cutter contacts. It is important to note that these failed particles still remain their mass and velocity; they simply separate from the workpiece but continue to collide to one another.

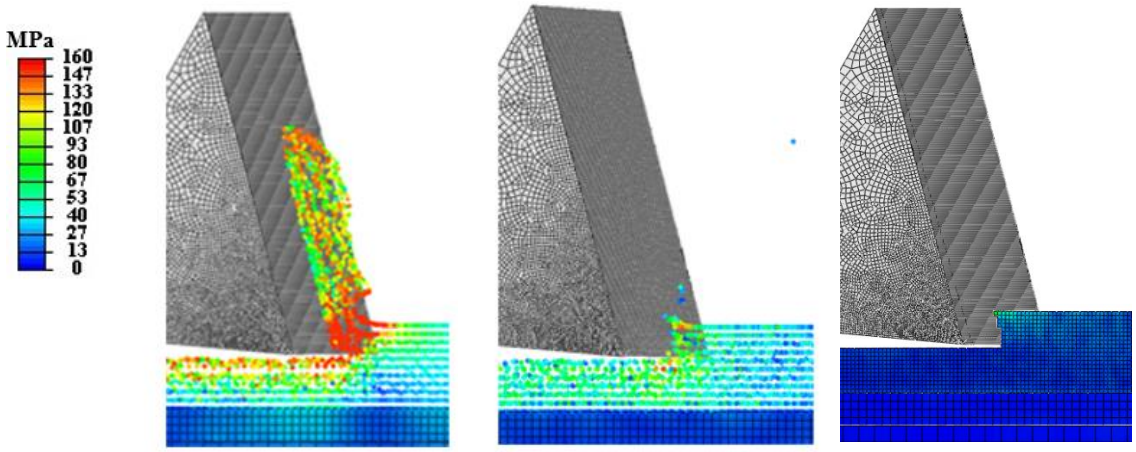

(a) (b) (c)

Figure 3-6. Effects of damage definition on the chip formation in the bone cutting simulation: (a) Undamageable SPH, (b) Damageable SPH, and (c) Damageable FEM; reprinted with permission from [3]

For the FEM case shown in Figure 3-6(c), the elements are removed from the model. Elements that have not reached the full degradation are also separated as debris

from the surface, while the majority of elements are completely deleted upon the cutter contact.

Figure 3-7 shows the specific cutting forces of these SPH and FEM models. Similar to the aluminum case (Figure 3-4), the damageable SPH tends to be easier to cut than FEM, while different from the aluminum case, the cutting force of the undamageable SPH is much higher than that of the damageable one because the natural separation occurs at a higher strain.

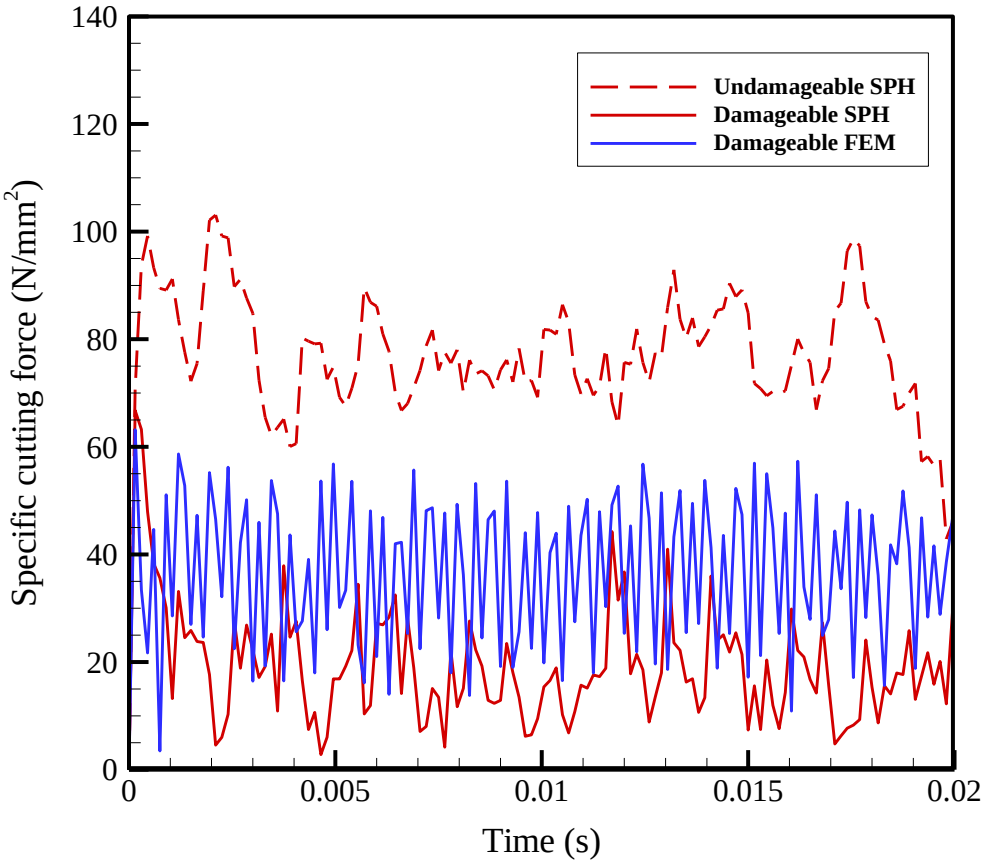

Figure 3-7. Effects of damage definition on the specific cutting force in the bone cutting simulation; reprinted with permission from [3]

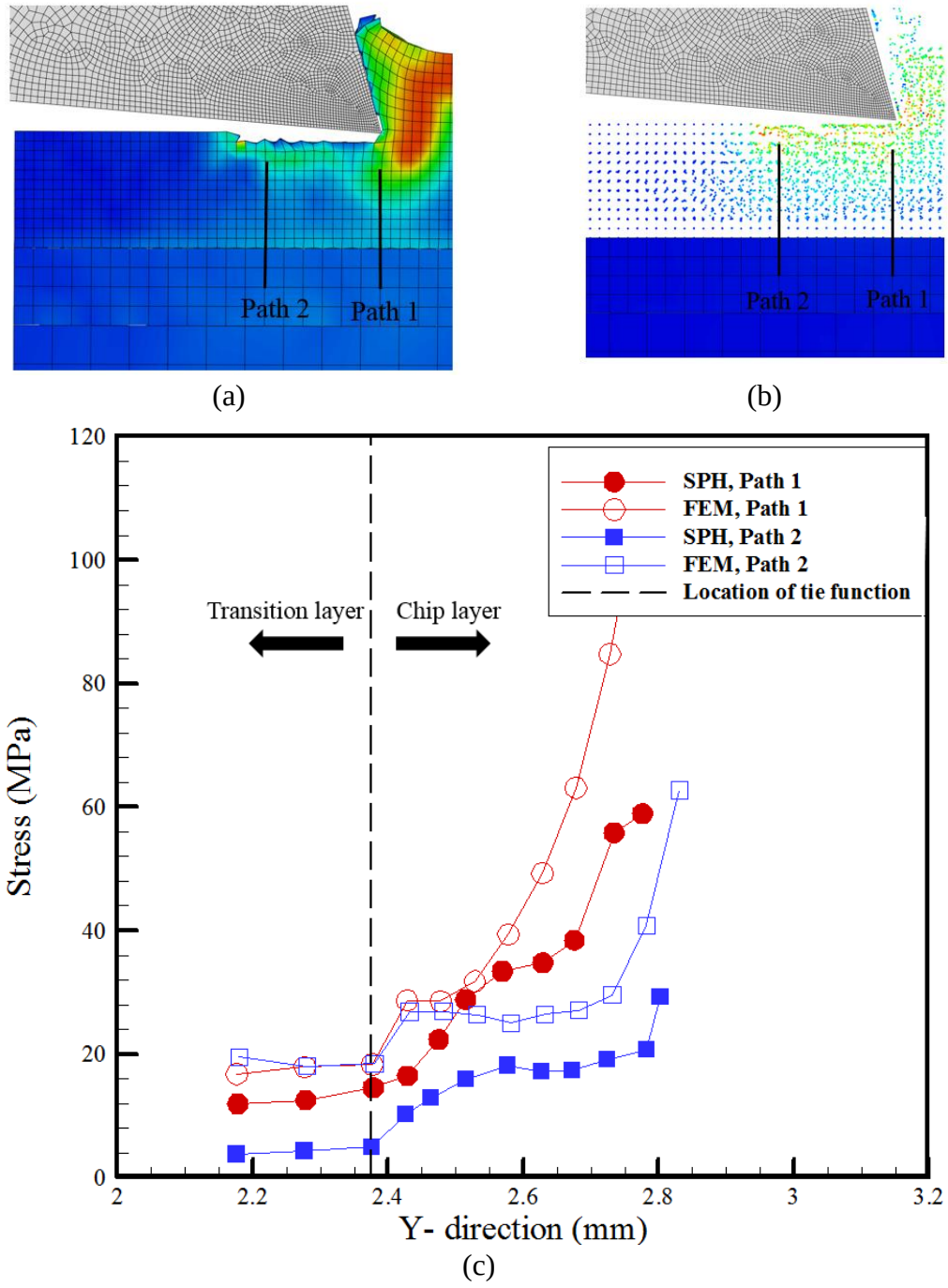

Figure 3-8. Stress variation along two designated paths, in the bone cutting simulation; reprinted with permission from [3]

Similar to the stress analysis in the aluminum cutting simulation, Figure 3-8(a) and (b) show the von Mises stress of FEM and SPH along *Paths* 1 and 2, respectively. FEM stress field is higher than that of SPH in the bone cutting simulation as well. The assumption of using the tie function to create an SPH/FE domain to decrease the computational cost is still valid, due to the smooth transition of stress across the interface as well as a small stress level, as shown in Figure 3-8(c).

3.3.2. Effects of particle density

Convergence test of the mesh size is a common practice in FEM, but the size effect on SPH has not been well studied. This section investigates the effects of SPH particle density on the specific cutting force and chip formation for both types of materials. To this end, on the chip layer of the model (Figure 3-1), three levels of particle density were made with the particle spacing of 0.2 mm, 0.1 mm, and 0.05 mm, which were named Coarse, Medium, and Fine SPH, respectively to represent their size with relative to DOC (0.4 mm). According to the last section demonstrating that the damage criterion must be defined for SPH cutting simulations, all the results of this section were obtained under a damage definition. Also, the presented results corresponded to the medium particle density.

3.3.2.1. Simulation results of aluminum cutting

Figure 3-9 shows the chip morphology resulted from FEM and SPH with all particle densities captured at the same time step. The converged FEM simulation, shown

in Figure 3-9(a) is capable of producing the curled chip. In contrast, the chips are always straight in SPH, regardless of the particle density, as can be seen in Figure 3-9(b)-(d).

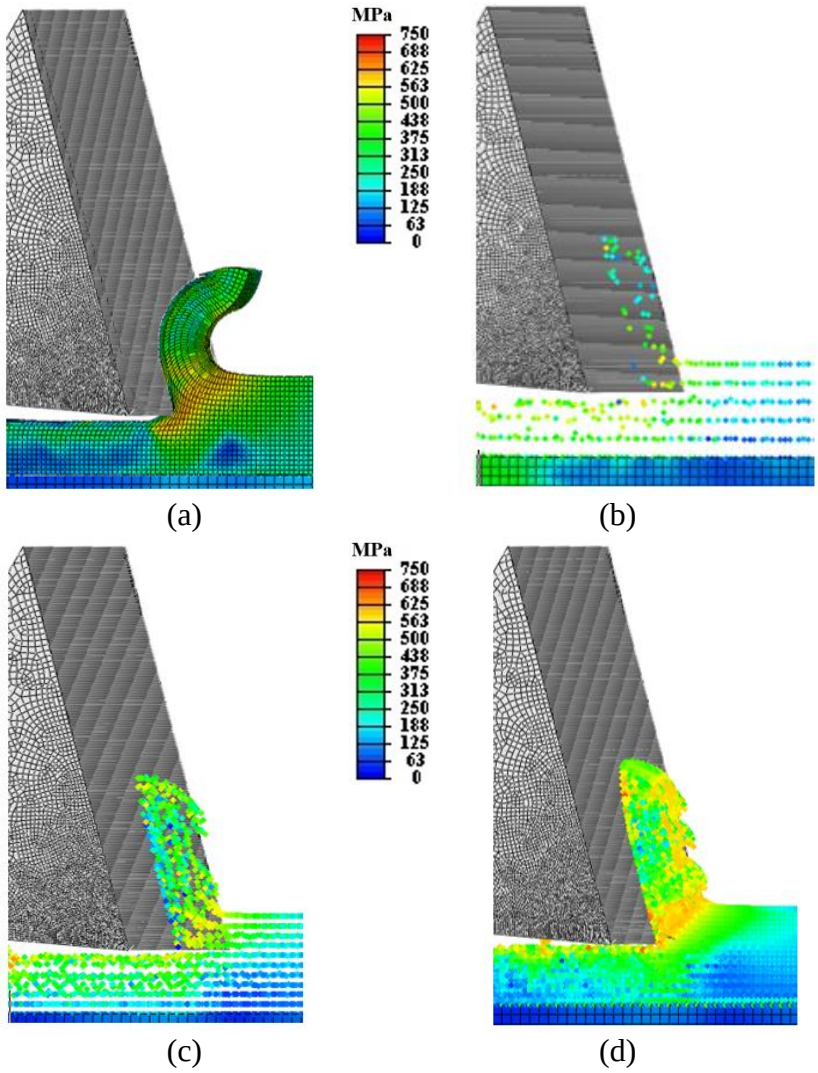

Figure 3-9. Chip formation of the aluminum cutting simulation of (a) FEM; and also SPH with three different levels of particle density: (b) Coarse, (c) Medium, and (d) Fine; reprinted with permission from [3]

This observation is in accordance with [69, 80, 92]. The straight chip could be due to the nature of this computational method as well as numerical limitations. These limitations will be thoroughly discussed in the next section.

The specific cutting forces associated with these cases for the aluminum are shown in Figure 3-10(a). The SPH simulation with coarse particle density produces the most oscillating force profile. Since the particle spacing is relatively large, sudden separation of a group of particles causes intermittent contact between the tool and workpiece, leading to a periodic force drop. In general, a higher particle density yields a smoother force profile. To investigate the convergence rate of SPH versus FEM, the equivalent FEM models were made with coarse, medium and fine meshes. In Figure 3-10(b), the average FEM forces resulted from the coarse, medium, and fine meshes are 279 N, 353 N, and 388 N, respectively. These values were calculated by the average of the cutting force data from 0 to 0.015 s. The corresponding SPH forces are 396 N, 269 N, and 250 N, respectively. FEM and SPH have different convergence trends. The finer FEM mesh, the higher force is obtained. This is because of a reduced chip volume due to losing elements with a coarse mesh. Conversely, for SPH, the finer particle density, the lower force is obtained instead. This is due to the fact that, in a coarse mesh, particles can interpolate to a larger chip size because each particle represents a large volume (defined by the characteristic length). Also, unlike FEM, SPH does not lose volume although the particles separate from the workpiece.

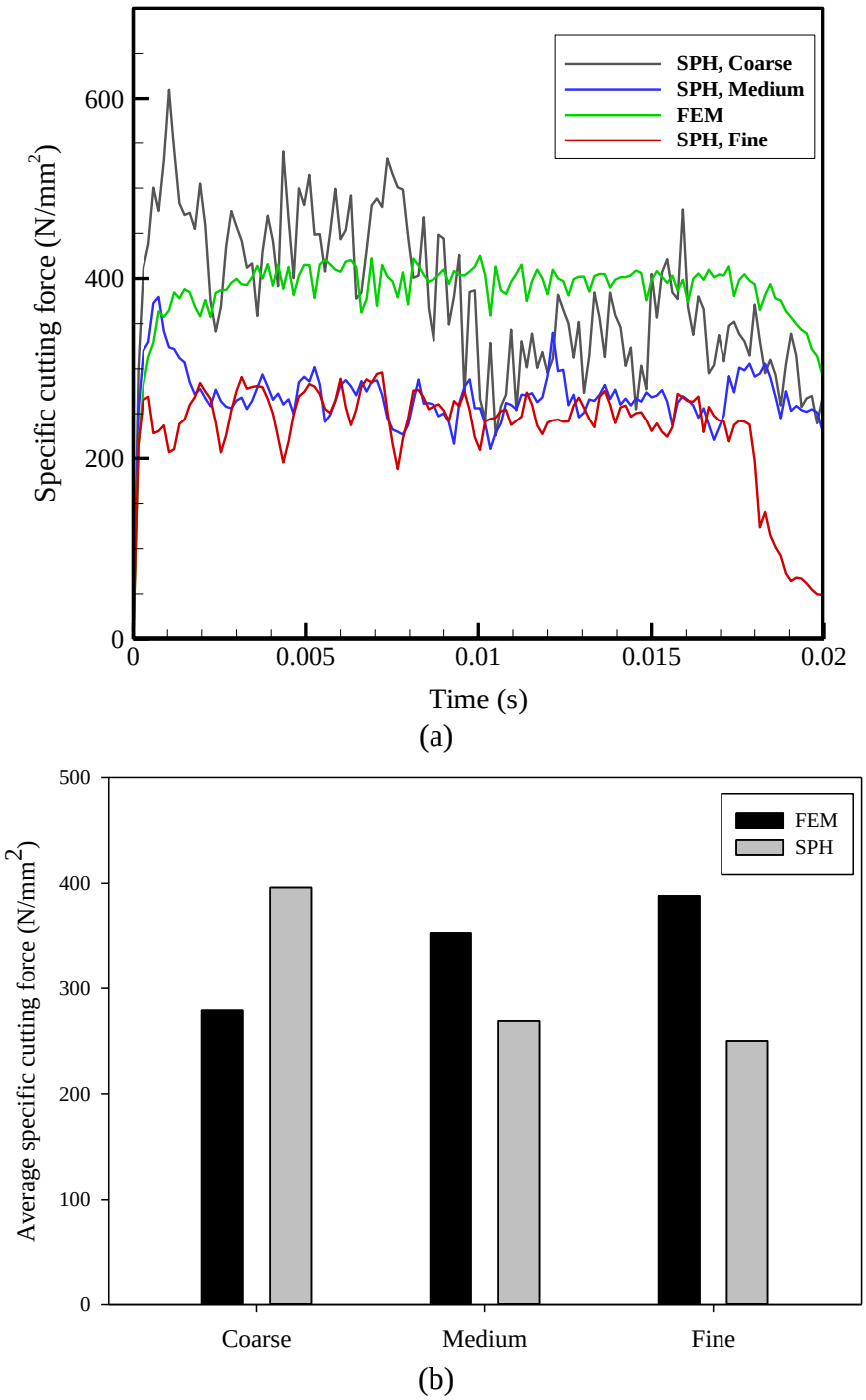

Figure 3-10. Effects of particle density on (a) the variation of the specific cutting force, and (b) the average specific cutting forces of FEM and SPH, in the aluminum cutting; reprinted with permission from [3]

For FEM simulations by commercial packages like ABAQUS, there are techniques such as distortion control, hourglassing control, the ALE adaptive meshing algorithm (Arbitrary Lagrangian-Eulerian) that can aid convergence. In this study, none of those techniques were used to ensure a fair comparison between FEM and SPH.

3.3.2.2. Simulation results of cortical bone

Similar to results for aluminum, SPH results of three particle densities for cortical bone are presented in Figure 3-11. The FEM case, which is shown in Figure 3-11(a), demonstrates a small piece of debris separated from the surface. Because deletion of elements in a fine mesh weakens the chip stiffness, the chip can break apart easily under an excessive deformation near the shear plane. In particular, the brittle damage causes the elements to lose their stiffness so rapidly that prevents them forming a continuous chip. The chip formation of SPH cases can be found in Figure 3-11(b)-(d). In coarse-density SPH simulation, although the failed particles are not shown, they are still in the computation with their mass and volume. The fine density case shows a similar chip formation to the FEM. However, it encountered an intense numerical instability after a few time steps. This issue will be discussed in the next section.

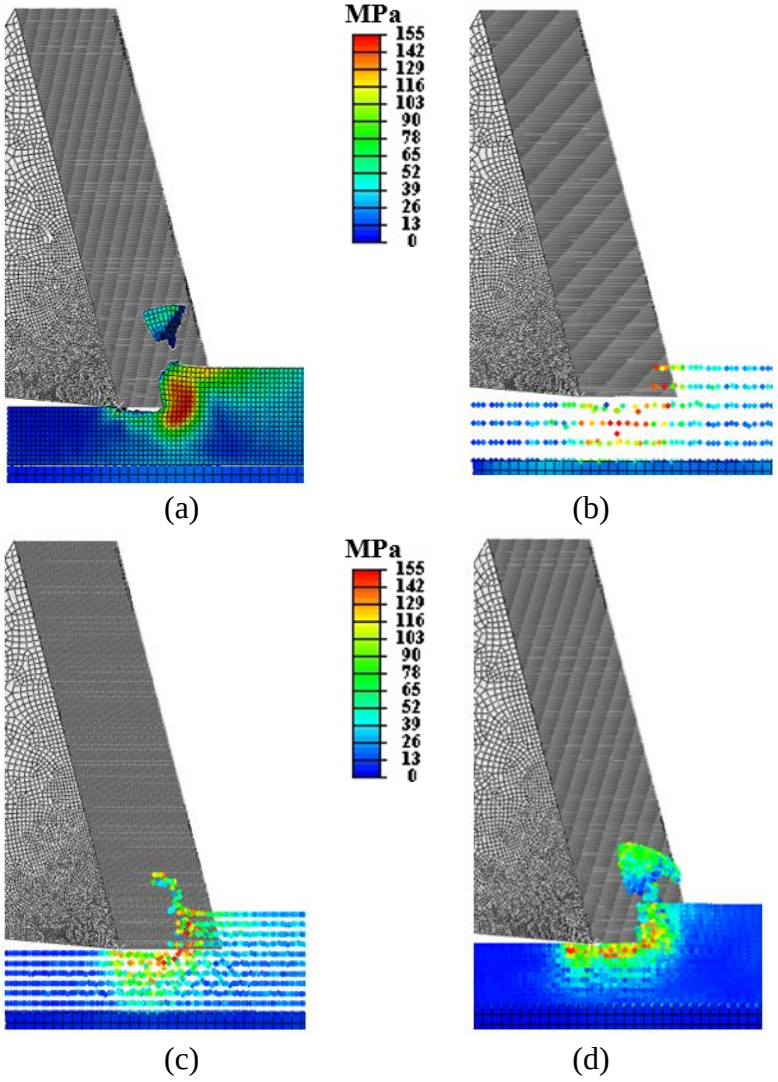

Figure 3-11. Chip formation of the bone cutting simulation of (a) FEM; and also SPH with three different levels of particle density: (b) Coarse, (c) Medium, and (d) Fine; reprinted with permission from [3]

The average specific cutting forces of the coarse, medium and fine SPH are 41 N and 20 N, 18 N, respectively. The corresponding FEM forces are 22 N, 37 N, and 47 N, towards the finest mesh. A similar trend of convergence to that of the aluminum results were observed for brittle cutting simulations.

3.4. Discussion

SPH could be an alternative to FEM in machining simulations, in particular for relatively brittle materials and locally large distortion with a coarse mesh. However, it is important to understand the discrepancies and limitations of SPH. To further explain the natural separation behavior, Figure 3-12 shows a hypothetical material model when the damage is defined and undefined in SPH and FEM. An undamageable FEM model shows an increasing stress until the excessive element distortion crashes the computation; an undamageable SPH can enable material failure when the natural separation occurs at $\bar{\varepsilon}_n$. This point is related to the smoothing length set in the SPH algorithm. In ABAQUS, this length is automatically defined to include 30-50 particles, which is about 1 to 1.5 particle spacing, at the beginning of the analysis and kept as a constant throughout the computation. This implies that a local strain over 100% could initiate natural separation since the nearest particle starts to fall outside of the kernel region.

Therefore, if no damage is defined in SPH, the cutting force could be either under- or over-estimated depending on the occurrence of natural separation at $\bar{\varepsilon}_n$ against the actual material failure strain, $\bar{\varepsilon}_f$. In the aluminum cutting, the force of the damageable SPH being less than the undamageable one implies a higher strain at the natural separation than the actual failure strain. Further, natural separation does not take into account the progressive damage of the material (*i.e.*, damage evolution), which can lead to a large force variation in the profile due to an intermittent material failure, as can be seen in Figure 3-4.

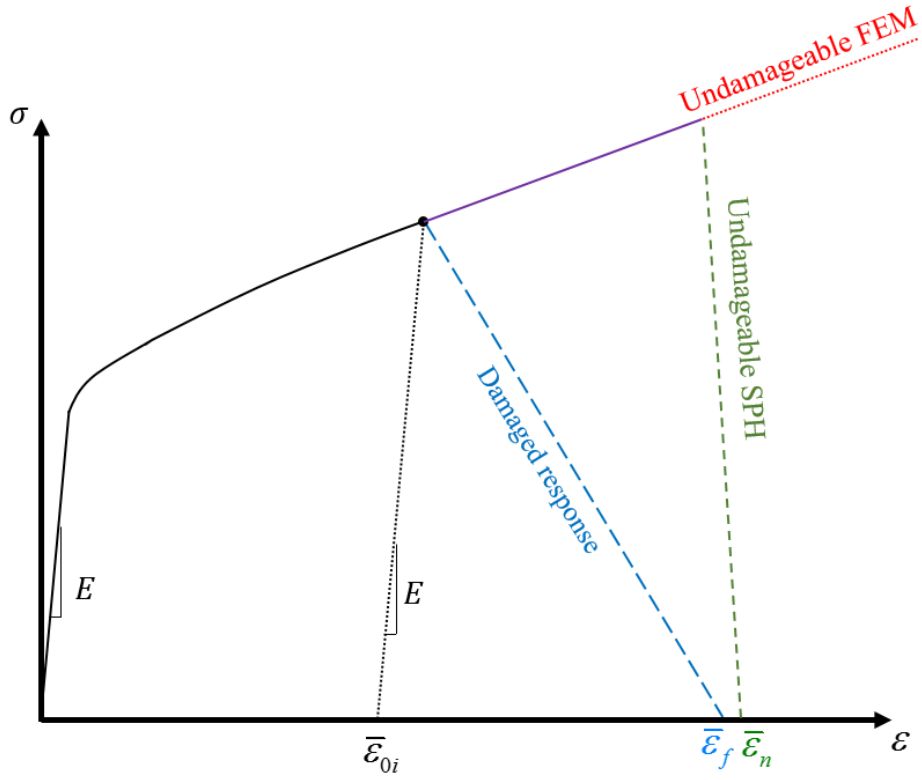

Figure 3-12. A hypothetical stress-strain curve that describes the behaviors of SPH natural separation, damageable and undamageable responses; reprinted with permission from [3]

In Figure 3-13, the fine SPH case is shown to become unstable after a few time steps due to the numerical instability. Such instability, often referred to "tensile instability," is exclusive to SPH that is not present in FEM [80, 93, 94]. This instability manifests itself as a clumping of particles, which consequently leads to artificial fracture or fragmentation [34]. Sometimes, the detached particles can aggregate and blow apart [93]. Figure 3-13(b) evidences the local fragmentation of the chip with a large number of detached particles. In this particular case, since the strain energy releases at a sudden after

rupture, these detached particles carry a high kinetic energy and can impact the neighboring particles that are still on the workpiece, leading to an early failure even before contacting the tool.

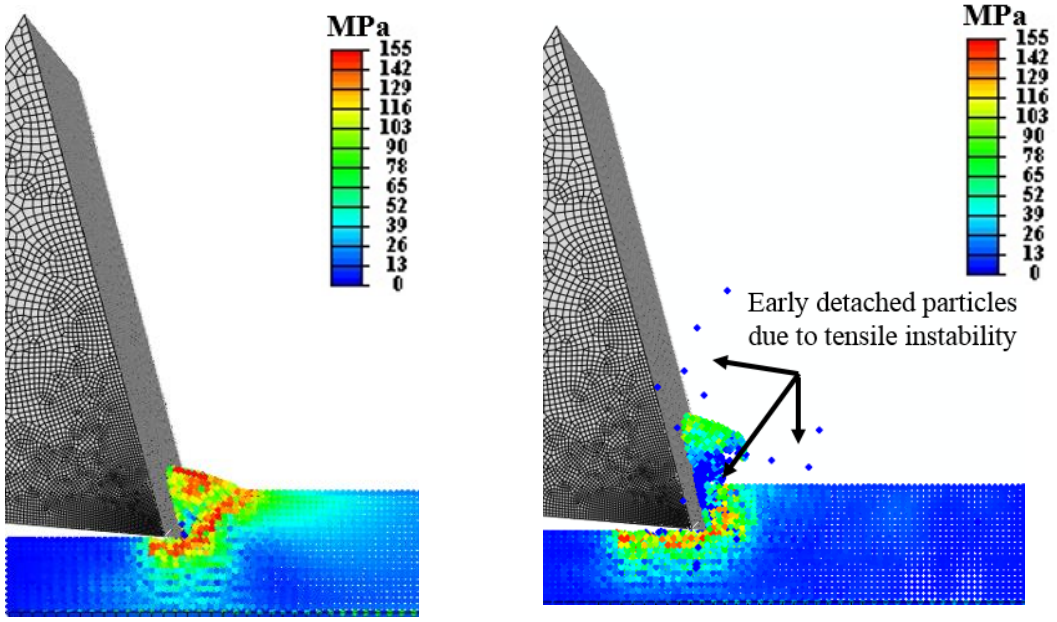

(a) (b)

Figure 3-13. An example of SPH instability around the shear band: (a) stable cutting with a continuous chip formation and (b) chip rupture and particles blow-up; reprinted with permission from [3]

For the chip morphology, SPH does not create a continuous curled chip as in FEM. This may be attributed to the boundary particles on the chip. SPH relies on interpolation from neighboring particles; however, due to the lack of neighbors, classic SPH approximation is not correctly calculated on the boundaries [80, 93]. This often leads to a higher field value on the boundary (e.g., stress and strain). There are a few developed methods to correct this deficiency, such as setting "ghost" particles around the boundaries

or adopting renormalization formulation [93]. Renormalization is another mathematical method that minimizes truncated Kernel functions on the boundaries.

3.5. Conclusion

FEM and SPH have both been applied to simulate machining processes, in particular that SPH is favorable for large-deformation problems. To further understand the interchangeability between these two methods, an orthogonal cutting process was numerically investigated in this study on ductile and brittle materials, respectively. It should be mentioned that experiments are not conducted for verification since this work aimed at emphasizing the differences between these methods and their effects on the simulation outcomes. As far as the model accuracy is concerned, a validation study is needed when either method is applied to a real material. The major conclusions are summarized below.

The effects of damage definition on the chip morphology and cutting forces demonstrated that appropriate damage criterion must be taken into account for SPH cutting simulations, despite the natural separation of particles, and regardless of the ductility of the material. A mechanistic model was presented to calculate damage initiation and evolution. Further, SPH produced less fluctuating force profile than FEM because of no sudden element loss (deletion) during cutting. This is particularly beneficial for simulating relatively brittle materials. However, SPH produces lower forces and stress than FEM; SPH cannot accurately capture curled chip in ductile materials.

Although SPH is feasible in machining simulations, underestimated forces and numerical issues with boundary particles and instabilities can lead to inaccurate prediction. A customized SPH algorithm would be needed to correct these issues. Given an increasing use of numerical methods in manufacturing processes, it is important to understand the limitations of SPH and thus apply it properly.

4. EMBEDDED COHESIVE ZONE FINITE ELEMENT METHOD*

Synopsis

This chapter[3] presents a fracture-based finite element method, named Embedded Cohesive Zone Finite Element Method (ECZ-FEM), to model brittle materials in machining. In ECZ-FEM, a network of cohesive zone (CZ) elements is embedded in the material body to capture undetermined crack initiation and propagation during a cutting process. The deflection of the CZ element is limited by a scaling factor to control the material ductility and chip formation. In conclusion, this model has demonstrated the potential to model cutting of brittle materials which are rigid and have no plastic deformation. However, the experiment for model validation is still required, which will be presented in the next chapter.

4.1. Introduction

Machining of brittle materials such as ceramics, rocks, carbon fiber reinforced polymers and bones is very common in aerospace/automotive industries and medical applications [95]. Although some efforts [49, 50, 96, 97] have been made to model machining of brittle materials, there is not a generalized method that can successfully emulate the physics behind brittle cutting – the instantaneous crack initiation and

[3] Content of this chapter has been submitted as: B. Takabi, B.L. Tai, "Modeling of Brittle Materials Cutting by Embedded Cohesive Zone Finite Element Method."

propagation upon tool-workpiece contact. Unlike ductile material cutting dominated by shear deformation across the shear plane, brittle material cutting is driven by fractures. Finite element method (FEM) has been widely used to simulate ductile material machining (e.g., metals) using Johnson-Cook plasticity model for cutting forces and chip formation [22, 98, 99]. However, FEM has not yet been successfully applied to brittle materials because of the difficulty to capture numerous and unpredictable cracks at the same time [6]. To do so, FEM needs an extremely fine mesh to simulate stress concentration and consequent element failure at each time increment, which can be time-consuming and computationally expensive [3].

To deal with fracture problems, researchers have developed the cohesive element which forms the cohesive zone (CZ) in a FEM model. The cohesive zone concept links the microstructural failure mechanism to the continuum fields [100]. A CZ element can begin to separate based on strain energy release rate, which often defined by a traction-displacement relationship. The cohesive zone-finite element method (CZ-FEM) has been a popular tool to investigate interfacial fracture problems. Examples include crack tip propagation, adhesive strength between two materials, and modeling of composite delamination [49, 96, 97].

Though not many, CZ-FEM has been used to solve machining problems of composites and ceramics. Rao et al. [49] simulated the orthogonal cutting of unidirectional carbon fiber reinforced polymer and glass fiber reinforced polymer composites using CZ between the fibers and matrix. They used a 2D plane-strain model and zero thickness cohesive elements to enable fiber detachment when the interfacial energy exceeds the threshold

defined by an exponential traction-displacement relationship. Umer et al. [96] used CZ-FEM to simulate metal matrix composite machining. They modeled the orthogonal machining of SiC particle-reinforced aluminum-based metal matrix composites by placing CZ elements between the particles and the matrix. A bilinear traction-displacement profile was used for CZ elements with zero thickness. Dong and Shin [47] developed a multi-scale model for simulating the machining of alumina ceramics in laser assisted machining. Zero-thickness CZ was assigned around the ceramic grain boundaries and the traction-displacement profile was determined based on a separate Molecular dynamics (MD) simulation. Note that CZ is often modeled as zero thickness because it is an imaginary interface inside the material in these cases, unlike physical adhesives.

In the above-mentioned CZ-FEM works, the CZ elements are placed either at known interfaces or paths as a pre-determined condition where cracks will initiate and propagate [101]. Therefore, CZ-FEM seems not possible for a homogenous, flaw-free brittle material in which potential cracking path cannot be defined. To address this issue, the current study proposes using a CZ mesh together with a regular element mesh to enable a network of potential cracks. A zero-thickness CZ element is embedded between regular elements. In other words, this CZ mesh will force the material to fail between elements instead of within an element. This modified CZ-FEM is named embedded cohesive zone finite element method (ECZ-FEM).

ECZ-FEM is somewhat similar to mesh-free methods such as smooth particle hydrodynamics (SPH) or discrete element method (DEM) in the sense of element separation rather than deletion. These mesh-free methods do not require a gridded domain

like FEM, so they are suitable for large deformation problems [65]. SPH has been used by a few researchers in metal cutting simulation [37, 38, 63, 68]. However, there are discrepancies among these works, especially on damage definition. Takabi et al. [3] investigated SPH in orthogonal cutting and showed the uncertainty of damage due to particles losing connection to each other (i.e., the natural separation), which can drastically change the outcomes. The separation is also not determined by fracture toughness but the material strength. Therefore, mesh-free methods cannot be an alternative to ECZ-FEM.

The ECZ-FEM for brittle machining is developed in this chapter using the commercial FEM software ABAQUS. In the rest of the chapter, Section 4.2 details the model configuration. Section 4.3 shows model development. Section 4.4 presents the results showing the effects of damage criteria and the scaling factor. Conclusions will be drawn at the end of this section.

4.2. Model Configuration

This section presents the overall configuration of ECZ-FEM, step-by-step procedures to construct the model, and the required modification for material properties. The model introduced here is built based on the corresponding orthogonal cutting experiment which will be presented in the next chapter.

A two-dimensional orthogonal, plane-strain cutting model is configured in Abaqus (version 6.14-2), as illustrated in Figure 4-1. There are two main sections in this model. The top section (named the chip layer) is the ECZ domain where CZ elements are embedded all around the main elements. The bottom section is the regular finite element

domain without CZ elements. This configuration saves the computational time from a fully embedded CZ model since the bottom layer does not directly involve in the tool-workpiece interaction. Instead, the bottom layer provides the compliance to the material during cutting. To ensure the stress continuity, the nodes on both sides of the interface must be merged or tied with all degrees of freedom. For this reason, the mesh sizes on both sections must match to have a perfect node-to-node alignment.

Table 4-1 shows the actual model dimensions used for two depths of cut (DOC), 0.1 mm and 0.3 mm. The boundary of the bottom layer is fixed in both translational directions (X and Y). The element size, *d*, is set at 0.01 mm. The bottom layer is meshed structurally with brick elements, while for the top layer, the elements are tilted by 45˚. The inclined elements are necessary because the maximum shear stress to fracture the material is expected to be around 45˚ based on the Merchant's Circle [102]. This configuration can avoid numerical instability when no CZ mesh aligns with the preferred fracture direction. The main elements are the four-node plane strain elements CPE4R, and the CZ elements are the four-node two-dimensional cohesive elements COH2D4. To embed zero-thickness CZ elements, all elements and nodes of the chip layer need to be assigned through the input file directly because each CZ element shares nodes with adjacent two main elements, as shown in Figure 4-1. The CZ element is defined by nodes ABCD, in which A and B belong to the element on the left side while C and D belong to the right side. Since these two pairs of nodes are overlaid geometrically, they cannot be identified from the graphic user interface. The mesh process is automatized by a separate MATLAB code.

Table 4-1. The model setup for different depths of cut (DOC)

	DOC (mm)	L (mm)	H (mm)	W (mm)
Case 1	0.1	2	0.5	0.1
Case 2	0.3	5	0.85	0.1

A complete mesh is imported to Abaqus/explicit to set up other boundary conditions. The plain strain thickness of 3 mm is also applied to the model to be consistent with the actual samples thickness. The cutting tool is modeled as a rigid body with a constant speed at 10 m/min to match with the experiment. The tool has a rack angle of zero, a clearance angle of 7˚ and an edge radius of 11µm.

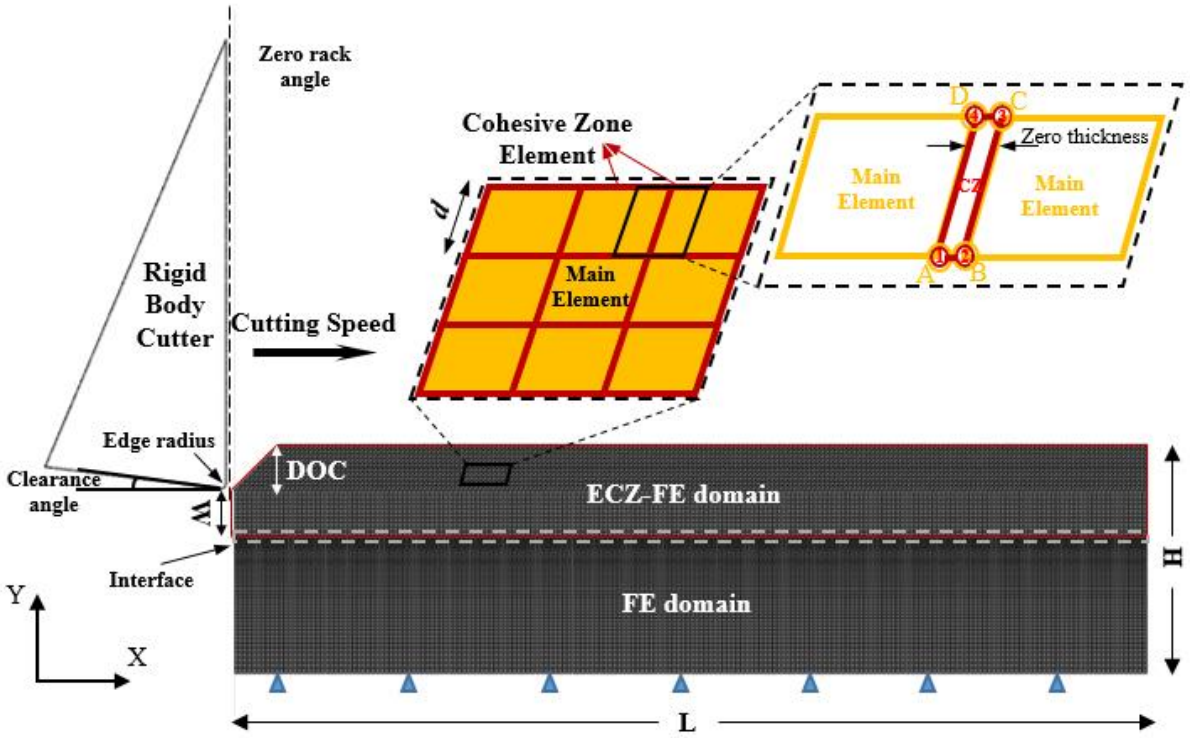

Figure 4-1. The schematic of the model configuration, boundary conditions, and element arrangements

4.3. Model Development

To develop a complete model as described in the last section, different steps have taken to investigate the effects of important parameters. In this section, the development of the model including trial and error was described step by step until the complete model was achieved.

4.3.1. Element size

The initial model was built by the element size of 0.01 mm (d = 0.01 mm), as can be seen in Figure 4-2 and a finer mesh, d = 0.005 mm, as shown in Figure 4-3.

Figure 4-2. The initial model with the original mesh size, d = 0.01 mm

Figure 4-3. The initial model with the finer mesh, *d* = 0.005mm

Figure 4-4 shows the chip formation in these two cases. The chip formation looks similar in both cases, while the software terminates the run in the first few steps. So, to reduce computational cost, the final model was considered to have $d = 0.01$ mm, while the model still needs to improve in other aspects.

4.3.2. Element configuration

The original element configuration was a simple structured quad element. Using this element type for an orthogonal cutting simulation might lead to a stress propagation through the chip layer, as can be seen in Fig 4-5. That is due to the CZ elements limitations that cannot deform properly to capture the maximum shear stress at 45˚.

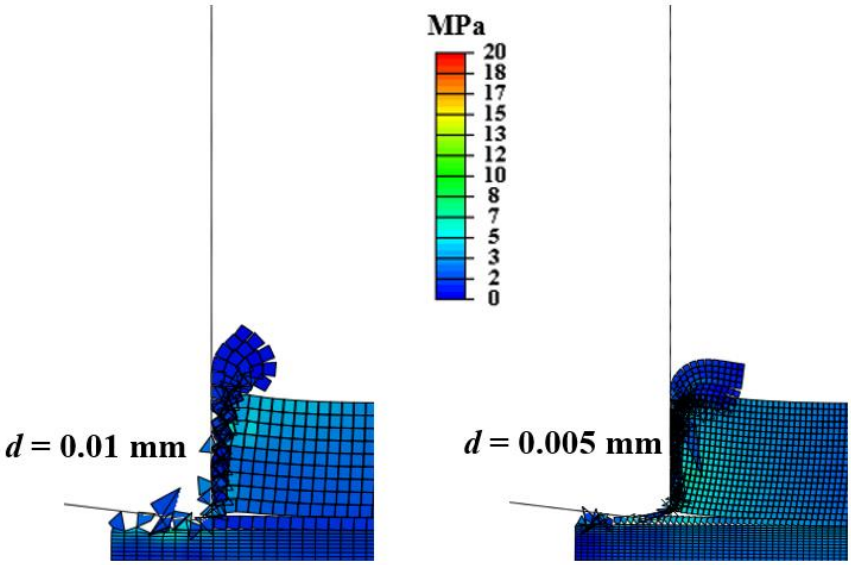

Figure 4-4. The chip formation resulted from the simulation with *d* = 0.01 mm and *d* = 0.005mm

Given the zero rack angle, the maximum shear stress resulted from fracture most likely occurs at 45˚ according to the Merchant's Circle [102]. So, the CZ element just passes on the stress to the next element, then a stress wave propagates throughout the body. To resolve such numerical instability, the elements were inclined by 45˚, made a parallelogram. Now, the CZ direction aligns with the fracture direction and that avoids stress propagation. So, for the final model, the element configuration was chosen to be 45˚ inclined.

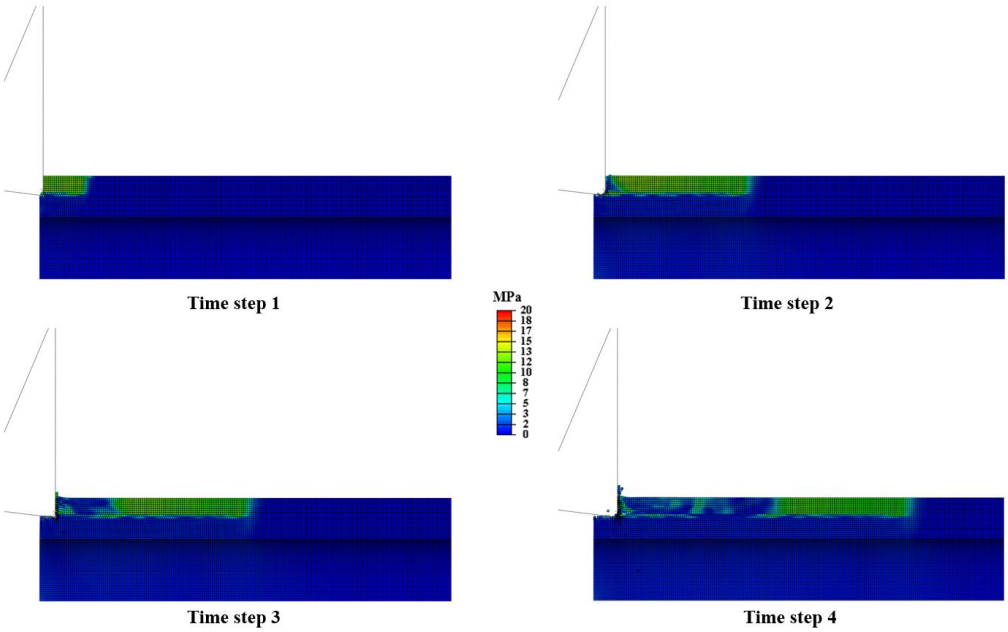

Figure 4-5. Stress propagation during the simulation

4.3.3. Mass scaling

To speed up the simulation, there is an option in Abaqus, named the mass scaling. In explicit dynamics simulations, the time step is internally calculated to provide a stable solution. Mass scaling increases the time step by scaling up the density in some small elements which control the time step. In this study, dealing with the zero-thickness CZ elements might significantly increase the running time. In order to reduce the computational cost, a mass scaling was adopted, after ensuring the independency of the results. Figure 4-6 compares the cutting force profile under different mass scalings. It shows that using the mass scaling up to 50 would not change the cutting force noticeably.

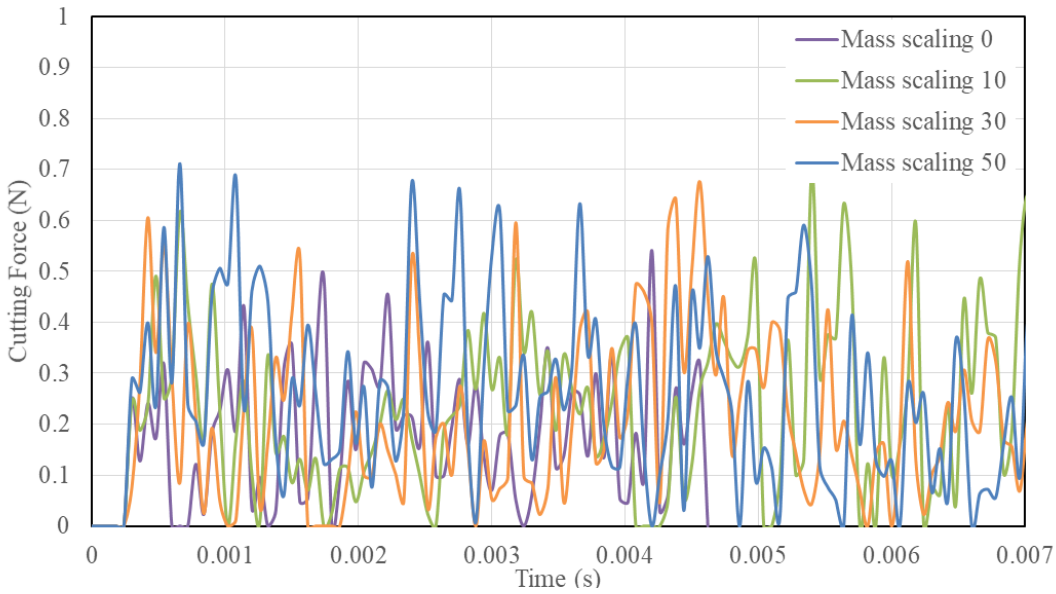

Figure 4-6. The effect of mass scaling on the cutting force profile

Figure 4-7 shows the effects of mass scaling up to 50 on the chip formation. The results show that all the cases are able to capture the shear band as well as small debris. The chip formation of all look similar. So, for the current research, the mass scaling of 30 was selected.

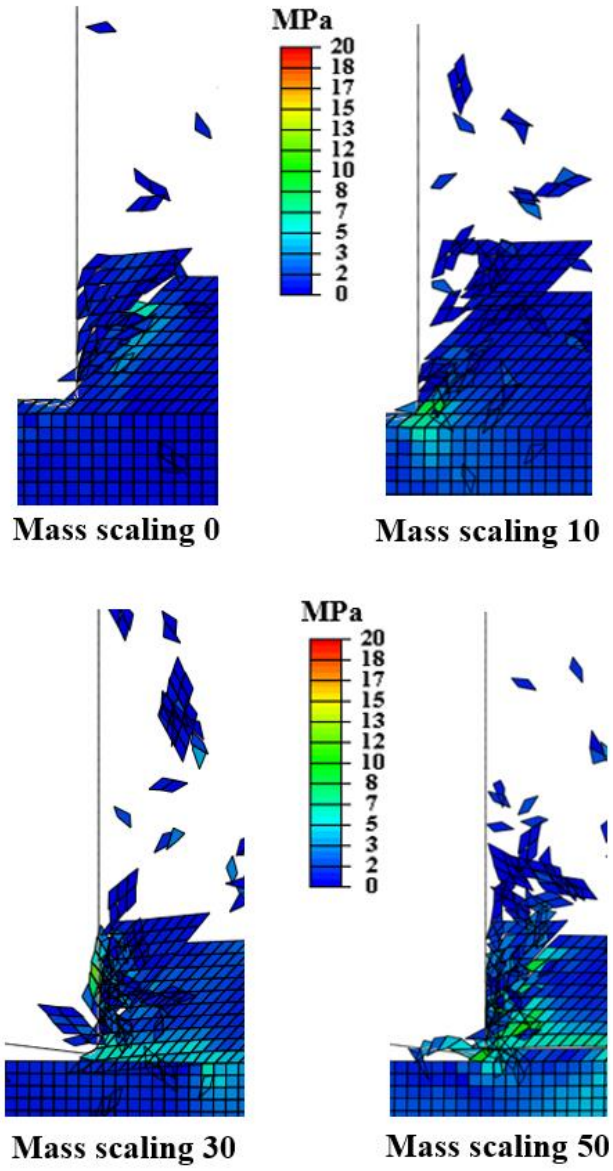

Figure 4-7. The effect of mass scaling on the chip formation

4.4. Results and discussion

This section investigates the critical factors that should be taken into account to build a successful ECZ-FEM model for brittle materials cutting.

4.4.1. Damage criteria of main and CZ elements

To apply the ECZ-FEM to a brittle cutting process, the material properties of the main and CZ elements and their damage criteria are defined separately despite being within the same entity. Assuming an isotropic material, the main element is defined by the modulus of elasticity (E), the ultimate strength, and damage criteria of the material. Although the model is meant to impart fracture-based failure on the CZ mesh, the main element should still allow to fail to avoid excessive element distortion when no fracture occurs. For this reason, the damage to the main elements is defined by an initiation at the ultimate strength followed by a progressive damage evolution by the Hillerborg's fracture energy theory. The total energy required to completely degrade the element after the damage initiation is G_f, which can be calculated from the material's fracture toughness K_c by Eq. (4-1):

$$G_f = \left(\frac{1-\upsilon^2}{E} \right) K_c^2 \tag{4-1}$$

The degradation is in a linear manner [71], such that

$$D = \frac{\bar{u}}{\bar{u}_f} \tag{4-2}$$

where $\bar{u}$ is the equivalent plastic displacement; $\bar{u}_f$ represents the equivalent plastic displacement at failure. The plastic displacement at failure is calculated by

$$\bar{u}_f = \frac{2G_f}{U_t} \tag{4-3}$$

where U_t represents the ultimate stress. These steps are standard when applied to metal cutting simulation along with the Johnson-Cook model.

The properties associated with the CZ elements embedded in the chip layer are defined differently. The cohesive zone is a mathematical approach in which the work is done to overcome the energy needed to open a crack. This work can be described by a traction-displacement relationship, t-δ, as seen in Figure 4-8. Damage initiation is related to the interfacial strength, *i.e.*, the maximum traction t_c, on the traction-displacement relation and the area under the relation represents the fracture energy, G_f as defined in Eq. (4-1).

In this study, a common bilinear traction-separation law is adopted. The maximum traction t_c should be less than the ultimate stress, yet close to that to avoid triggering main element failure [100]. Hence, the 80% ultimate stress is used here. The initial stiffness k should be large enough to ensure the continuum between the two adjacent bulk elements, but small enough to avoid numerical issues such as spurious oscillations of the tractions in an element. Studies suggest that the initial stiffness of CZ elements can be calculated from Eq. (4-4), which balances accuracy and simulation stability [103, 104].

$$k = \frac{E}{d} \tag{4-4}$$

where E is the bulk elasticity, d is the maximum element size.

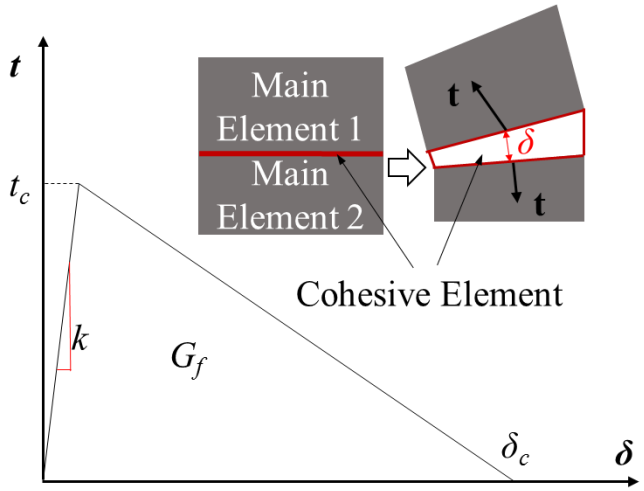

Figure 4-8. Bilinear traction-displacement of cohesive zone elements

The maximum deflection of a CZ element δ_c is determined by given G_f and t_c, as shown in Fig. 2. Therefore, the deflection can become larger than the element size when a fine mesh is used. A large deflection is impossible since it virtually increases the part ductility when a CZ mesh is embedded in the material. Because of this limitation, a scaling factor is introduced here to limit the maximum deflection to control the expansion of CZ elements and thus to control the chip behavior. However, when the deflection is scaled, the fracture energy is also scaled, which can affect cutting forces and other modeling outputs. This tradeoff has become a major concern in this modeling method.

To properly apply this model with the scaling factor, the following assumptions are made. No plastic deformation occurs in the material and all the force contributes to material removal. Friction is negligible. The specific cutting energy (energy required to remove a unit volume of material) is based solely on the fracture energy. Since the cutting

force (F_c) can be related to the specific cutting energy (p) and material removal rate (MRR), as described in Eq. (4-5),

$$F_c v_f = MRR \cdot p \tag{4-5}$$

the cutting force is linearly proportional to the specific cutting energy. This is, cutting force is scaled together with the CZ element's fracture energy. The simulated cutting force will be scaled back to estimate the actual cutting force. This concept will be validated in the experimental study.

4.4.2. The scaling factor, f

A scaling factor is necessary to control the maximum deflection of CZ elements and thus the part ductility. In the case of 30 pcf, the original CZ deflection goes up to 0.064 mm. With the adjacent element size being 0.01 mm, this allowable deflection is equivalent to a 600% elongation, which is unrealistic. Figure 4-9 shows four different scenarios when using the original G_f and scaled G_f that limits the deflection to be 0.00512 mm (51.2% elongation), 0.00128 mm (12.8% elongation), and 0.00032 mm (3.2% elongation), respectively. As seen in Figure 4-9 (a) with the original G_f, the workpiece and elements experience excessive deformation. Many stretched CZ elements remain alive though the chip has been distorted significantly. Figure 4-9 (b) shows small but consistent debris generated from the shear plane, which is similar to cutting of brittle metals like high carbon steels. Figure 4-9 (c) starts to generate irregular debris containing dusty pieces, which can be similar to ceramic or composite material cutting. Figure 4-9 (d) shows a more extreme

case, where the workpiece shatters upon the tool contact. From this simple example, it can be seen that a fairly small scaling factor is needed in order to force the material to behave brittle. Note in the simulation no self-contact is employed because the elements are supposed to support each other via CZ elements. Self-contact might also exponentially increase the computational load due to the larger number of surfaces involved in the contact algorithm.

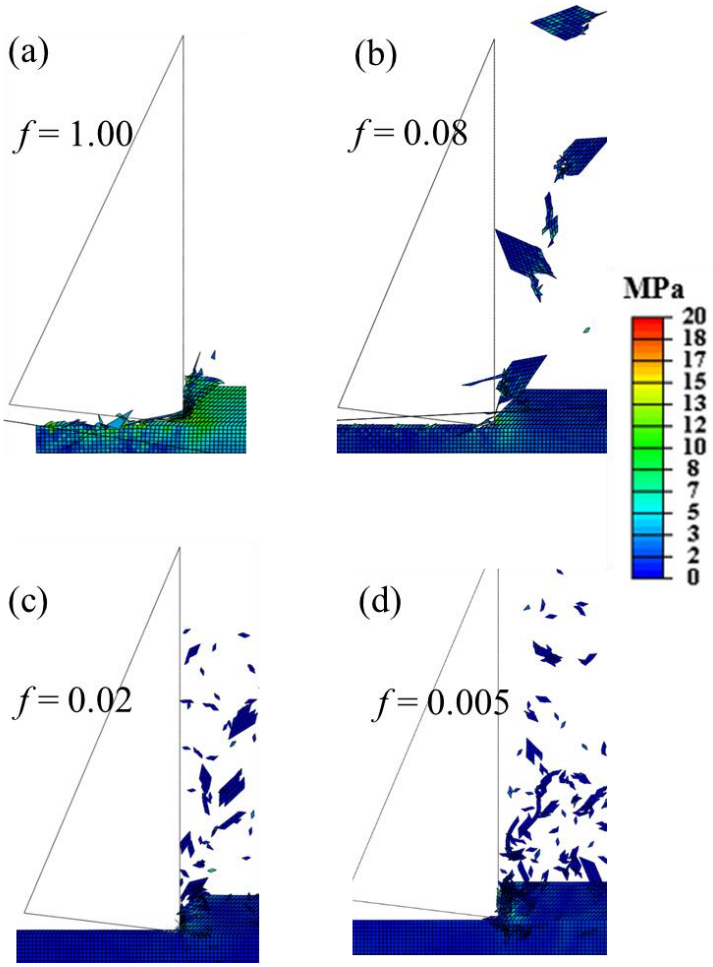

Figure 4-9. Material response to the cutting tool with different scaling factors (a) f = 1, (b) f = 0.08, (c) f = 0.02, and (d) f = 0.005

4.5. Conclusion

This chapter presented a fracture-based model for brittle material cutting using cohesive zone concept, namely ECZ-FEM. In this model, a network of cohesive zone elements is embedded in the material body to allow free development of cracks to emulate the undetermined fracture during a cutting process. The model configuration was described and different critical parameters to develop a successful model were investigated. The results show that ECZ-FEM can be a great approach to model the cutting of though and stiff brittle materials which possesses no plastic deformation. To limit the maximum deflection of CZ elements though, a scaling factor was introduced. Different scaling factors could generate different chip formation. Hence, an appropriate scaling factor should be chosen through model calibration against experiment. The details will be discussed in the next chapter.

5. MODEL VALIDATION AGAINST EXPERIMENT*

Synopsis

The ECZ-FEM model was completely setup in the last Chapter. The model is validated by an experimental study in terms of chip formation and cutting forces with two different brittle materials and depths of cut. The experimental setup[4], material selection and the model validation is presented in this chapter. For chip formation, ECZ-FEM can capture dusty debris, irregular chips, and unstable crack propagation as seen in the experimental cases with a properly selected scaling factor. For the cutting forces, the relative differences among these cases are similar in both simulation and experiment, but the model prediction is always higher by 30-50%. Limitations of this model are discussed towards the end of this chapter. In conclusion, this model has demonstrated the applicability to brittle materials that are rigid and have no plastic deformation.

5.1. Introduction

Orthogonal cutting is the most basic cutting configuration for all machining processes. The essential geometrical parameters include rake angle, clearance angle and the depth of cut. To validate the proposed ECZ-FEM model which was developed in the last chapter, a set of experimental tests was designed. Several literatures [105-108] have

[4] Content of this section has been submitted to B. Takabi, B.L. Tai, "Modeling of Brittle Materials Cutting by Embedded Cohesive Zone Finite Element Method."

done experiments on an orthogonal cutting test and the setup has become common such that it needs to capture the chip formation and find the cutting force. The selected materials for this study are two bone-mimetic foams and a full 2×2 factorial test is carried out, on two different materials and depths of cut (DOC).

The first section in this chapter includes the orthogonal cutting setup by which chip formation and cutting force can be obtained. Section 5.2 explains the material selection and material properties for this study. Section 5.3 shows a comparison between the numerical results obtained from the ECZ-FEM against the corresponding experimental data. The last section shows the experimental setup and the method to find the fracture toughness, K_c of the selected materials.

5.2. Orthogonal Cutting Setup

Prior to the orthogonal cutting tests for the current project, the testbed for the orthogonal cutting experiment was used for another study through a collaboration with Ecole Nationale Supérieure d'Arts et Métiers, ENSAM, France and Department of Industrial and Systems Engineering at Texas A&M University [108]. The study focused on machining natural fibers reinforced plastic (NFRP) composites. The setup used for that study was shown in Figure 5-1.

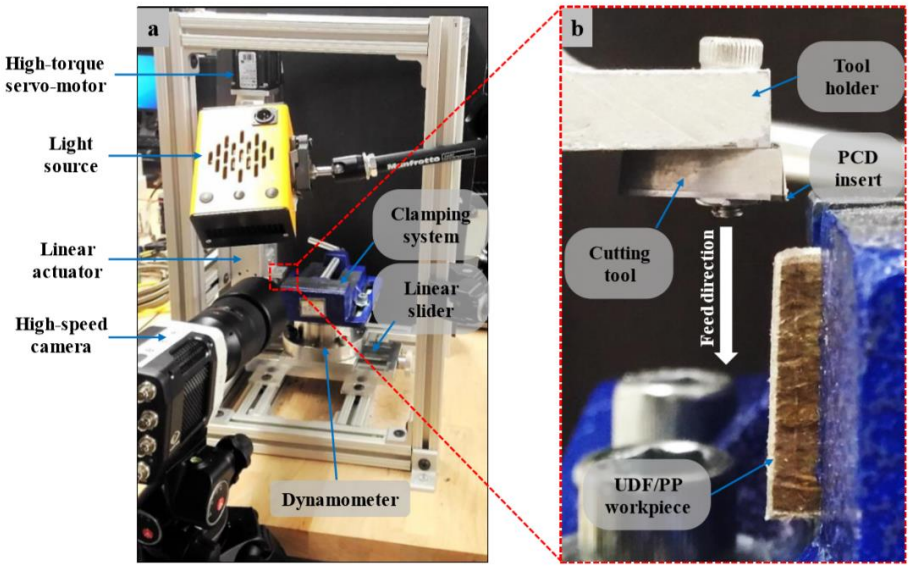

Figure 5-1. (a) The orthogonal cutting setup for machining of NFRP composites (b) The PCD insert position against the workpiece.

Through that work, the weaknesses of the setup which led to high vibration was recognized and the setup was improved for the current study, even though the cutting forces were expected to be in a lower order of magnitude. The strength of the structure enhanced, especially near the cutting zone, where the workpiece is placed, by replacing the vertical bars by titled bars. Besides, the horizontal linear actuator was replaced by one which has an automatic lock, minimizing the sample movement during cutting, i.e. the cutter/sample engagement. The setup for the current test is shown in Figure 5-2.

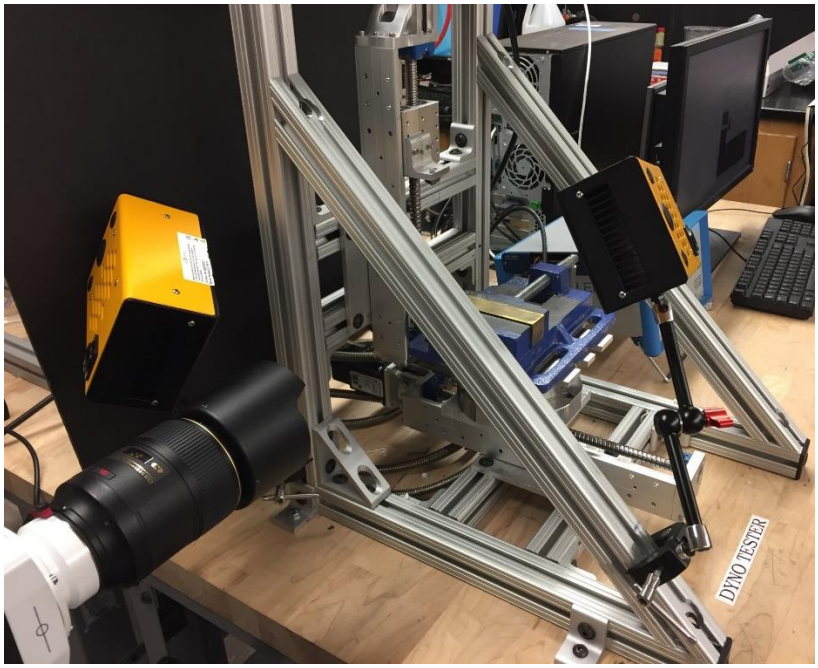

Figure 5-2. The orthogonal cutting setup for the current study

In this experiment, the solid foams, the 30 and 40 pcf, were sectioned to a 20×30×3 mm testing sample. Each sample's cutting surface was polished with the same grit size to ensure a consistent initial condition. Figure 5-3 illustrates the schematics of the experimental setup for the orthogonal cutting setup which consists of two linear actuators and a dynamometer for force measurement. The cutting tool is attached to the vertical linear actuator through a customized tool holder. The linear actuator (L70, Moog Animatics, Milpitas, CA) is driven by a high-torque servo-motor to maintain a constant feed rate during cutting. The force dynamometer (Model 9272, Kistler, Winterthur, Switzerland) is used to capture high-speed or high-frequency force data up to 5 kHz. Data collection is performed via an amplifier, a shielded connector block, and a data acquisition

device (PCIe-6321, National Instruments, Austin, TX), along with a data recorder, LabVIEW, at 2 kHz sampling rate. The workpiece is fixed by a clamping system on the top of the dynamometer which is placed on the other linear slider to control the depth of cut for each test.

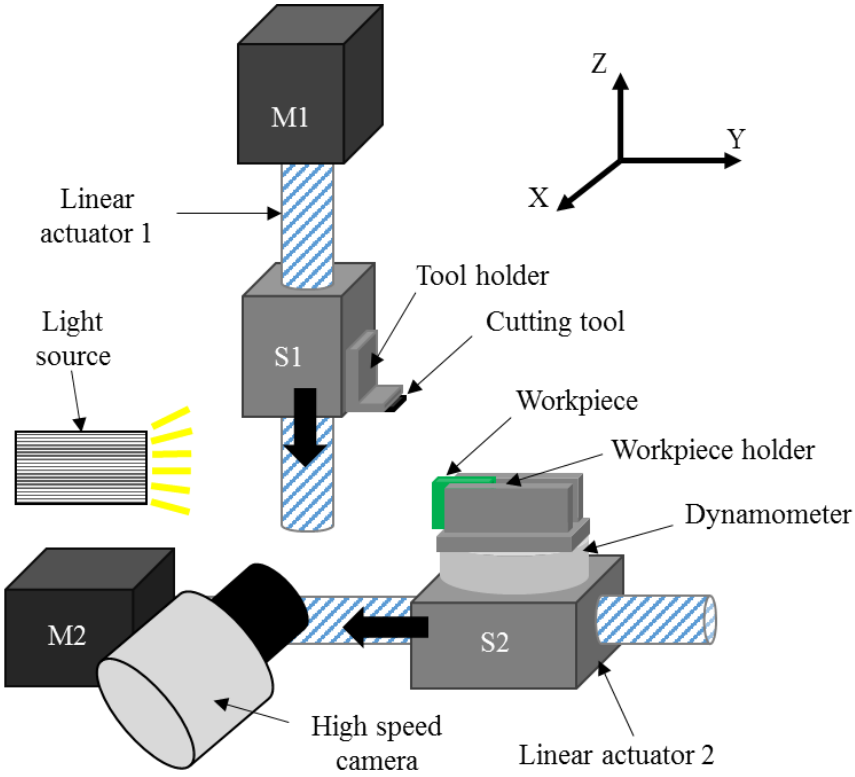

Figure 5-3. A schematic of the orthogonal cutting setup for model validation

The cutting tool has a tungsten carbide substrate and a polycrystalline diamond (PCD) insert as a cutting edge, provided by Sandvik (Model TCMW16T304FLP- CD10). This PCD insert is extremely hard to avoid any possible deformation or wear at the cutting edge. This cutting tool has a zero-rake angle and a clearance angle of 7°. The cutting edge

radius is 11μm, measured by a high-definition surface profiler (Alicona InfiniteFocus G4, Graz, Austria).

In this experiment, two depths of cut, 0.1 mm and 0.3 mm, are used to present common chip loads for a machining process. The cutting tool is moved at a constant velocity of 10 m/min also to represent a machining condition. This cutting speed is equivalent to a 3 mm drill running at 1061 rpm or a 10 mm cylinder being turned at 318 rpm. These parameters are applied to the two specimens and repeated for four times each.

5.3. Material Selection and Characterization

The brittle materials used for the experiment are two types of solid bone-mimetic materials made of high-density polyurethane (PU) foam (Sawbones, Vashon, WA). This material provides consistent and uniform material properties; it is isotropic and does not require a large force to cut. It is ideal for the modeling purpose and experimental validation without extraneous variables such as vibration, impact shock, and heat. These two foams are named based on their densities, 30 and 40 pcf (pound per cubic foot), which equal to 480 kg/m^3 and 640 kg/m^3, respectively. The 30 pcf has the ultimate strength of 12 MPa and the elasticity modulus of 592 MPa; the 40pcf has the strength of 19 MPa and the modulus of 1000 MPa, respectively [109].

To implement the damage criteria in the computational model, the fracture energy G_f was needed which could be calculated from the fracture toughness K_c. So, the fracture toughness of the foam was obtained through a three-point bending test, following the ASTM Standard D5045–93 shown in Figure 5-4. The actual experimental setup is shown

in Figure 5-5. Figure 5-6 shows the sample before and after the test. The fracture toughness K_c was calculated based on Eq. (5) [110].

$$K_{Ic} = \frac{3P_{max}S}{2BW^2}\sqrt{\pi a} f(a/W), \quad (\text{MPa mm}^{0.5}) \tag{5}$$

$$f(a/W) = 1.122 - 1.40(a/W) + 7.33(a/W)^2 - 13.08(a/W)^3 + 14.0(a/W)^4$$

where P_{max} is the maximum load in (N); a, B and W are specimen dimensions in (mm).

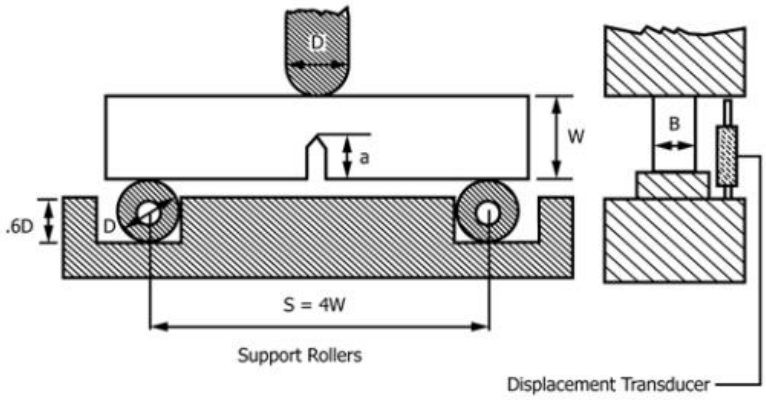

(a)

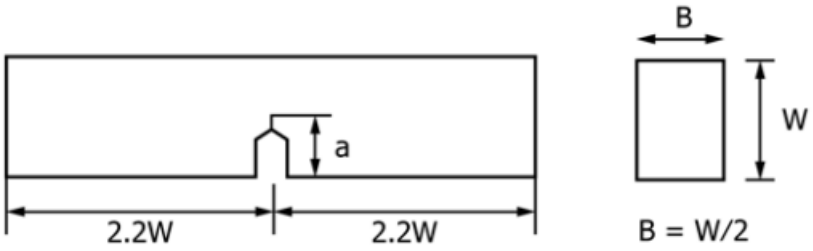

(b)

Figure 5-4. ASTM Standard D5045–93 to find the fracture toughness K_c (a) A schematic of the setup, (b) the sample

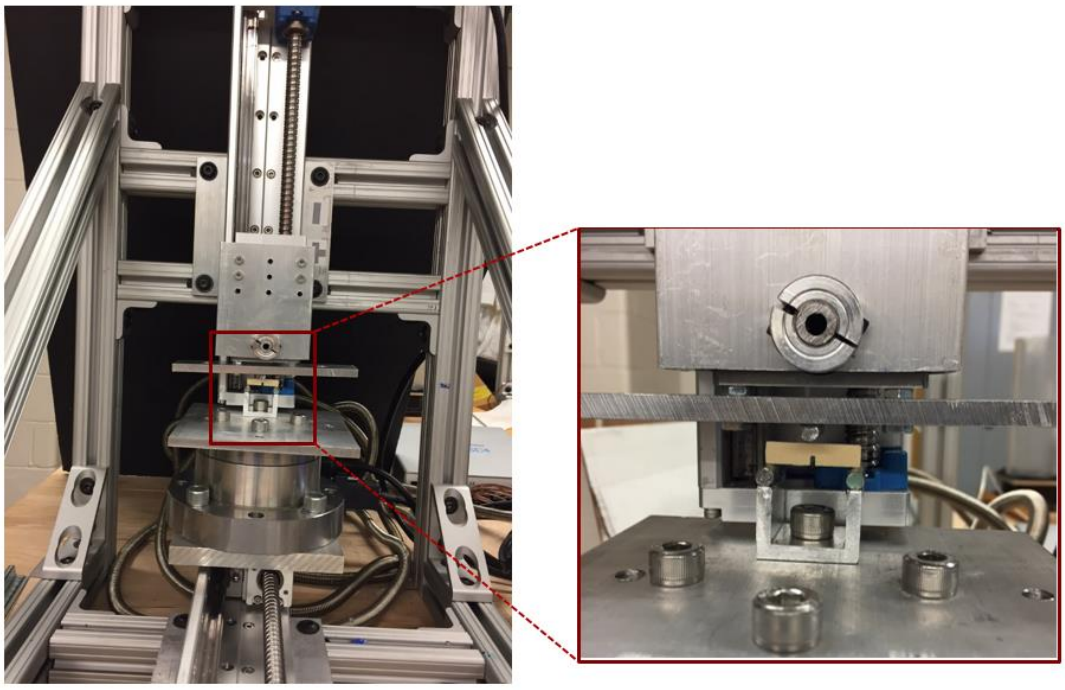

Figure 5-5. The three-point bending setup to find the fracture toughness K_c of the foams 30 and 40 pcf

(a)

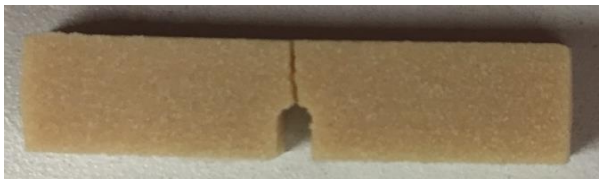

(b)

Figure 5-6. The sample for three-point bending experiment, (a) before, and (b) after the test

The averaged K_c for the 30 pcf is 0.46 MPa.m$^{1/2}$ and that of 40 pcf is 1.13 MPa.m$^{1/2}$. The 40 pcf is stiffer and also tougher than the 30 pcf. Based on these properties, the original CZ element properties are calculated in Table 5-1 below. As seen, the allowed cohesive element displacements are both larger than the element itself (0.01 mm).

Table 5-1. The CZ element properties for the testing materials 30 pcf and 40 pcf

Samples	t_c (N/mm^2)	k (N/mm^3)	G_f (N/mm)	δ (mm)
30 pcf	9.6	59,200	0.31	0.064
40 pcf	15.2	100,000	1.12	0.147

5.4. Simulation and Experiment Results

The simulations results are compared to the experiments in terms of the effects of the depth of cut (DOC) and material properties (30 pcf and 40 pcf) in this section.

5.4.1. Chip formation with a selected scaling factor

As discussed in Chapter 3, determining the scaling factor *f* is a critical step as it can affect the material behavior significantly. Figure 5-7(a) shows the simulation result of 30pcf at DOC = 0.1 mm with a selected *f* = 0.02 based on trial and error to match with the actual chip formation. The simulation can capture the irregular chips of different sizes generated from the cutting zone. Then, this scaling factor is used to simulate the case of 0.3 mm DOC. The result is shown in Figure 5-7(b). A larger DOC tends to generate bigger chips surrounded by small debris as compared to the case of 0.1 mm DOC. Consistently, the experiment also sees much bigger or clustered pieces when DOC increases to 0.3 mm. The results of 30 pcf with the selected scaling factor show good agreement between the model and experiment.

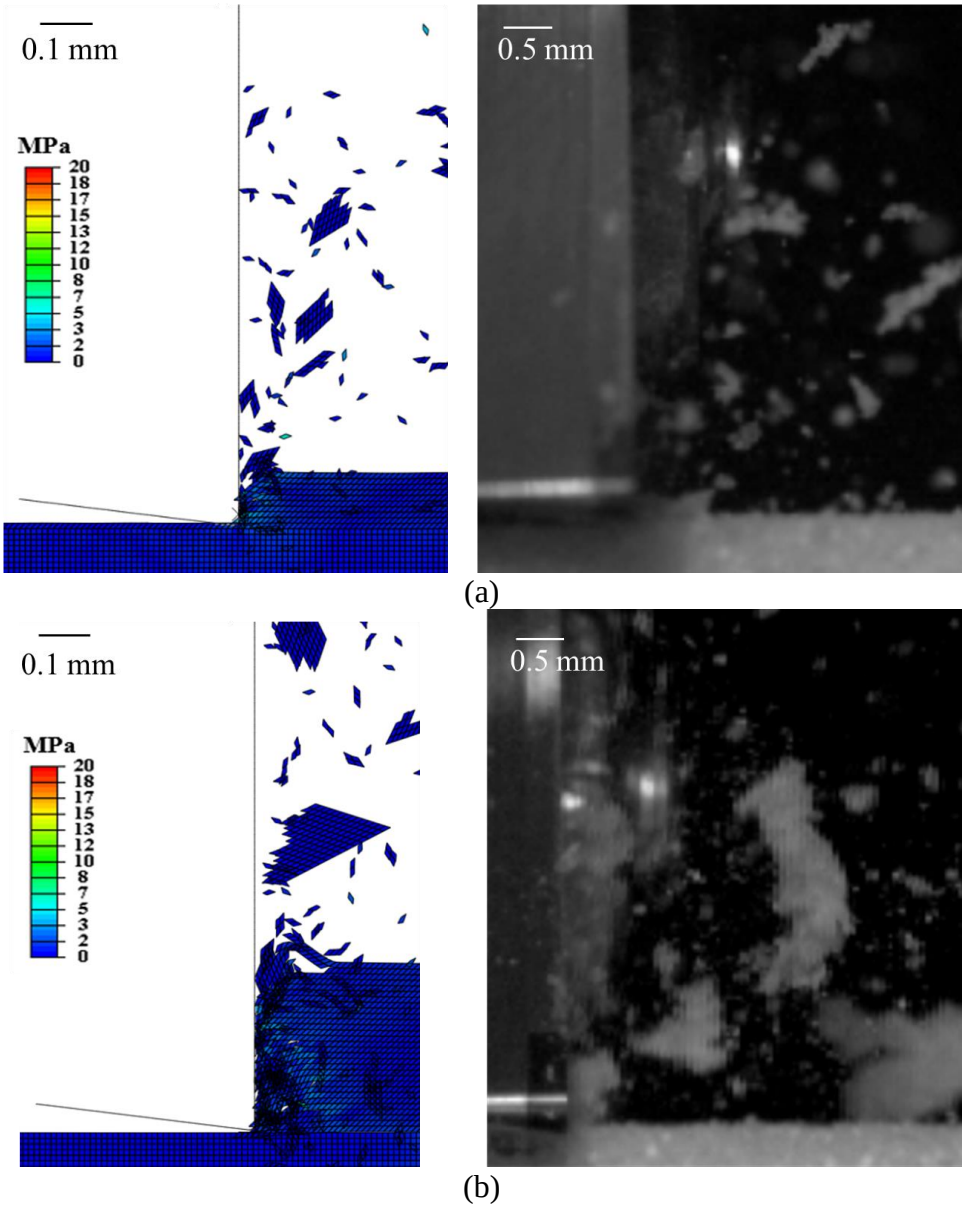

Figure 5-7. Chip formation of the 30pcf with (a) DOC = 0.1 mm and (b) DOC = 0.3 mm

For the 40 pcf, the same scaling factor of 0.02 is used not because of the 30 pcf. Instead, this scaling factor means the maximum of 0.00294 mm deflection (29.4% elongation), which is much more ductile than that of the 30 pcf (12.8% elongation). The simulation

result of 40 pcf at 0.1 mm DOC and corresponding experimental observation are shown in Fig. 6(a). Different from 30 pcf at 0.1 mm DOC, bigger and similarly-sized chips are generated with some dusty debris around. This phenomenon also indicates a more ductile behavior.

When the same scaling factor is applied to the case of 0.3 mm DOC, the simulation of the cutting process starts to show unstable chip formation, as shown in Figure 5-8(b) and (c) at different time steps. Cracks can propagate ahead of the cutting tool motion to generate large chips and sudden fracture along the cutting direction to shear the chip layer. This phenomenon is also seen in the experiment thought the unstable cracks into the workpiece cannot really be captured.

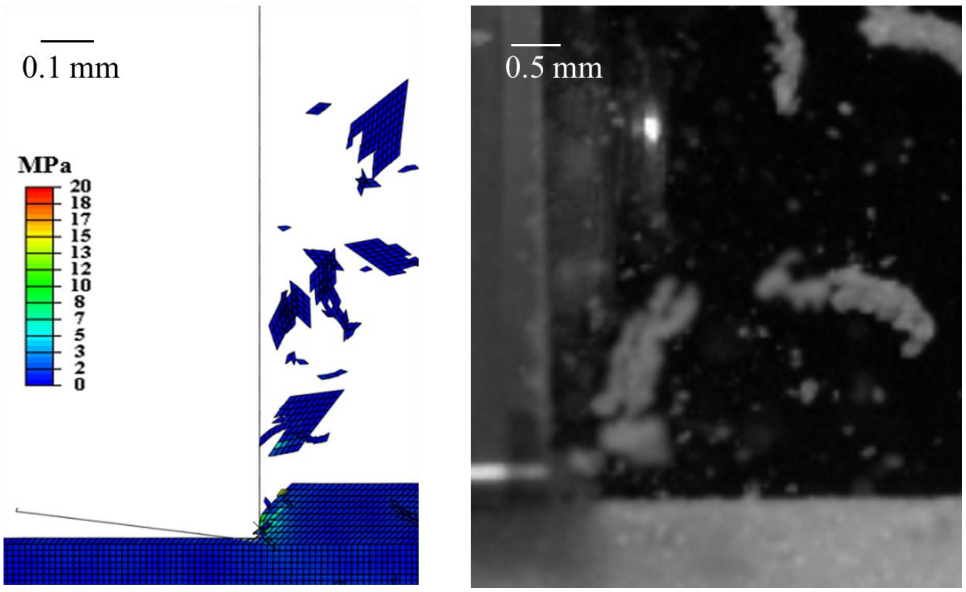

(a)

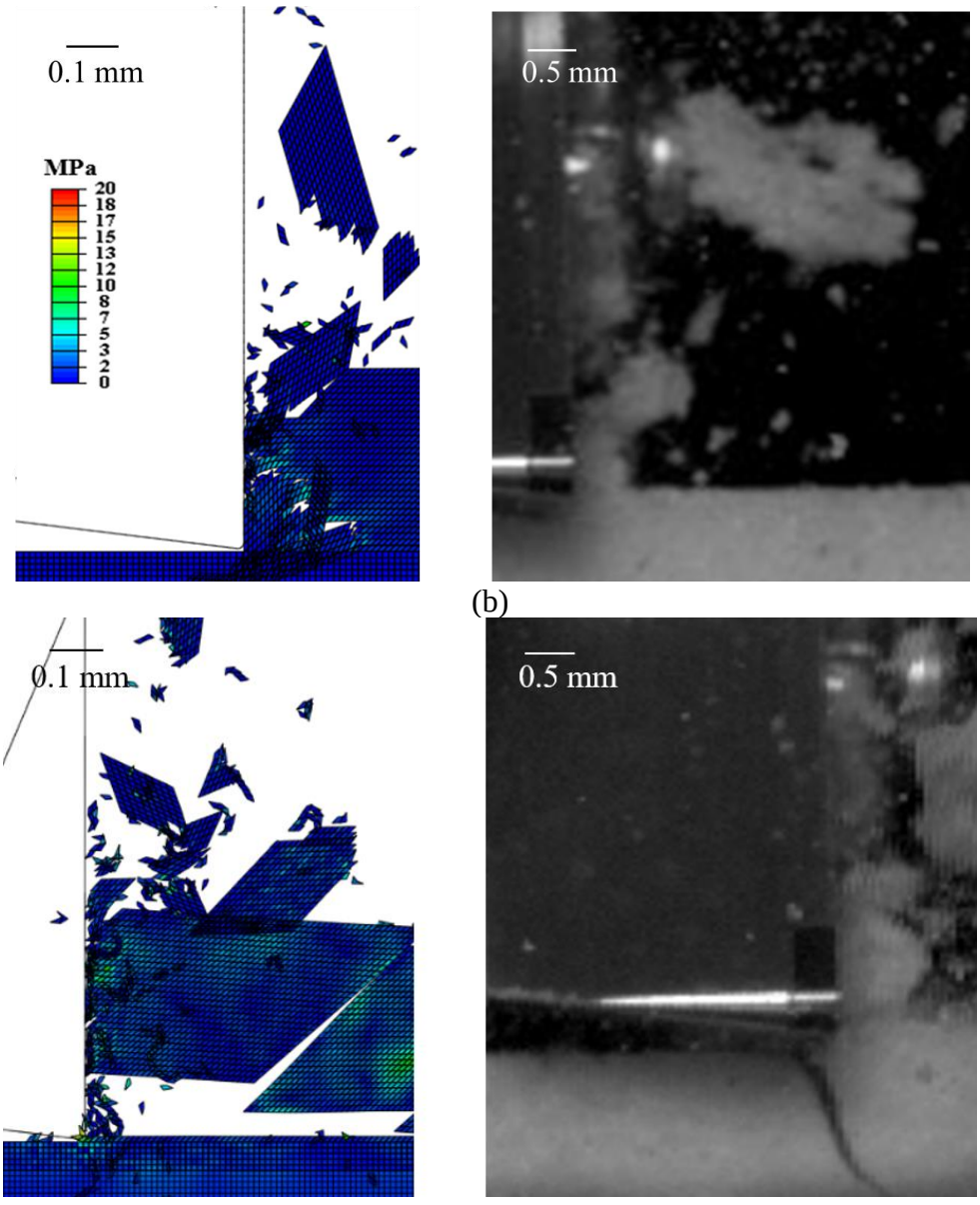

Figure 5-8. Chip formation of the 40 pcf with (a) DOC = 0.1 mm, (b) DOC = 0.3 mm, and (c) DOC = 0.3 mm at a later time step.

5.4.2. Cutting forces

Figure 5-9 shows the cutting forces measured from four repeated tests for 30 pcf at DOC = 0.1 mm. Force profiles are oscillating due to the brittle nature of the material. The system vibration is assumed minimal in these measurements as the cutting forces are very small (less than 20N) compared to the system rigidity. During a roughly 0.14 s cutting period, the cutting forces can reach and stay at a certain level, namely the steady cutting, and then decrease toward the end. The simulation length is about 0.01 s only since it is enough to reach the steady cutting to extract the force. According to the scaling factor f = 0.02 used in these simulations, the simulated force is scaled by 50 times ($1/f$) and overlaid on Test 4, shown by the comparison in Figure 5-9(b). Since the simulation ran at every 0.00006 s increment, the sampling frequency is equivalent to 16.7kHz as opposed to 2 kHz of the experiment. The averaged force of simulation is 12.51 N and the experimental average across the steady cutting is about 9 N. Although the forces are at a similar magnitude, the simulated force is oscillating much more significantly (0 to 35 N). These discrepancies may be attributed to the fact that CZ mesh is a discrete method to emulate a continuous material, so the force may experience more significant drop when a CZ element fails. Such discrepancy is seen in all simulation cases of 30 and 40 pcf at 0.1 and 0.3 mm DOCs.

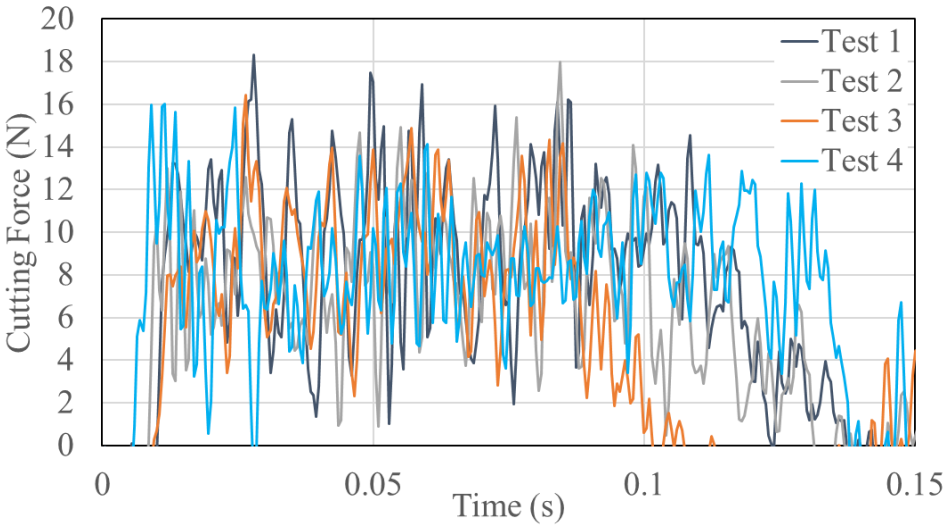

(a)

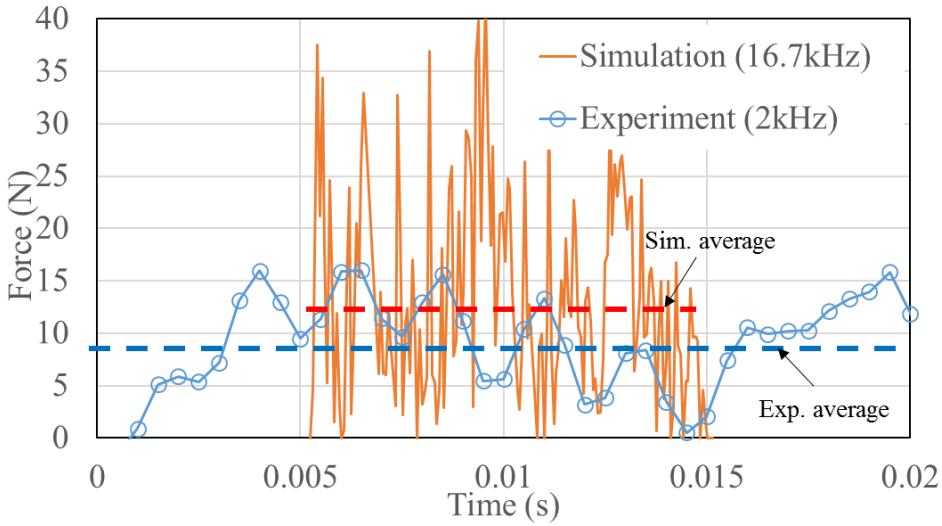

(b)

Figure 5-9. Experimentally measured cutting forces of 30 pcf at DOC = 0.01 mm and the comparison with the simulated, scaled cutting force.

To compare all simulated cases at a time, the average forces of experiments, from the steady cutting region, and the corresponding simulated forces are compared side-by-side in Figure 5-10, where the error bars stand for one standard deviation from the four replicated tests. Although the overall trends of prediction are correct, the simulated forces

tend to be constantly higher by 30 to 50%. This difference can be because of oscillating force profiles or the non-linearity of the scaling factor. Nonetheless, the simulation model is considered successful despite a large scaling factor needed to overcome the CZ element limitation.

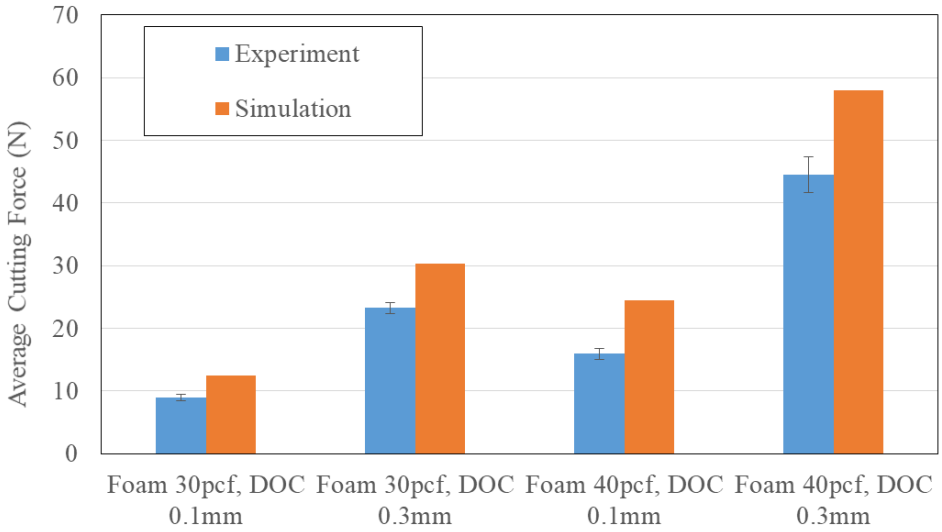

Figure 5-10. Comparisons between all simulated cutting forces and experimentally measured forces (averaged)

5.5. Discussion

In ECZ-FEM, the key to a reasonable result is choosing an appropriate scaling factor, *f*, by calibrating the model behavior. As mentioned, CZ elements are determined by a traction-displacement relationship. When CZ elements are embedded in the workpiece, their displacement can change the material ductility (elongation), and thus it must be limited. Figure 3 has shown how different scaling factors can change the chip formation from very ductile to brittle. Although limiting CZ deflection inevitably changes the material property (G_f), the effect on cutting force should be linear because of energy

conservation. Therefore, the calibration of model based on experiment is necessary with the current modeling method.

The model-predicted cutting force is consistently higher by 30-50% as shown in Figure. 8. This indicates that the fracture energy is always overestimated though the model predicts the relative behaviors well among different materials and depths of cut. This over-estimation can be explained by the difference between the static and dynamic fracture toughness, K_c. The fracture energy G_f is determined by the material toughness K_c, which is measured from a quasi-static test. Thus, the obtained K_c is a static fracture toughness while the actual dynamic toughness may be much lower, as reported in the literature [111, 112]. However, it is technically challenging to measure a dynamic toughness at a comparable speed of cutting (10 m/min or 167 mm/s).

Another model limitation is the significant oscillating force profile as shown in Fig. 7. This is because the model consists of embedded CZ elements which have different material properties and degrees of freedom from those of the main elements, the force can change drastically when the model experiences deformation and damage. Another reason could be a non-self-contact definition of the main elements, which results in intermittent contact between the tool and material and significant force drop. A much finer mesh with full contact definition may mitigate the problem at the cost of extreme computational time.

5.6. Conclusion

This paper presents a fracture-based model for brittle material cutting using cohesive zone concept, namely ECZ-FEM. In this model, a network of cohesive zone elements is

embedded in the material body to allow free development of cracks to emulate the undetermined fracture during a cutting process. The research results have shown a certain degree of agreement with the experiment in terms of chip formation and cutting forces while also revealed some limitations. Controlling the maximum deflection of the cohesive zone element through a scaling factor is a critical step in this method, and for that, an experimental calibration is necessary. This factor is currently determined on a qualitative basis because it is a behavior indicator instead of a property. Also, the current model is limited to brittle materials that do not have any plastic deformation in order to scale the force linearly with the fracture energy. The model should also not be used for flexible material because the CZ mesh does not have enough degrees of freedom to handle deformation. In summary, there is still room for the improvement of this model, including the CZ element itself, anisotropic material behaviors, temperature dependent properties, and overall accuracy.

6. CONCLUSIONS AND FUTURE WORK

6.1. Conclusions and major contributions

This dissertation studied the modeling of brittle materials cutting. Quantitative as well as fundamental understanding the mechanics of brittle materials cutting were achieved. The proposed methodology, Embedded Cohesive Zone Finite Element Method (ECZ-FEM) have demonstrated to be a good tool to model brittle materials cutting and reasonably predict the chip formation and cutting force. The particle-based method, Smoothed Particle Hydrodynamics (SPH), seems to be feasible to simulate brittle materials cutting, but it still needs further study and more method development.

Major contribution of this dissertation can be summarized as following:

I. The motivation for this study was to address an industrial need. Brittle materials machining is a common process in various industries from medical devices to aerospace. However, there is not a generalized and robust model yet that is capable of predicting the cutting behavior. To address the need, this study was to develop a model for brittle materials cutting.

II. The current study also includes a fundamental research. Even though brittle materials machining has been widely used in the manufacturing world, it is still one of the most difficult and challenging works for manufacturers, mainly due to lack of knowledge in brittle cutting mechanics. This dissertation focused on the mechanics of brittle materials cutting by

understanding the dominant cutting mechanism. The cutting behavior including the chip morphology and cutting force was also investigated.

Therefore, this study was can benefit both industry and scientific worlds.

The conclusions and important findings in this research can be summarized as follows:

1. The dominant mechanism of ductile materials cutting is shear stress band, while that of brittle materials cutting is fracture. As a result, brittle materials cutting deals with crack initiation and propagation.
2. Regular FEM cannot practically model brittle materials cutting, since it can hardly capture crack initiation and propagation. An FE model with an extremely fine mesh though might be able to capture the cracks, but it is not practical for complex problems due to the computational cost. So, other methods should be introduced to model brittle materials cutting.
3. SPH can be an alternative for FEM to model brittle materials cutting, because it eliminates the need for volumetric elements. So, it can handle large deformations. But to apply this method to brittle materials cutting, crucial parameters such as particle density and damage definition should be investigated.
4. SPH can neither capture curled chip in ductile materials cutting, nor predict precise cutting forces for brittle materials cutting, due to the numerical issues with boundary particles, natural separation of particles and instabilities. It can capture powder-like chips in some brittle materials

cutting though. To apply SPH to brittle materials cutting, the method should be improved by developing a customized SPH algorithm.

5. To model brittle materials cutting by both SPH and ECZ-FEM, appropriate damage definition should be taken into account. The implementation of damage definition in commercial software, Abaqus, is by including both damage initiation and damage evolution which can be calculated by the proposed mechanistic model.
6. The cohesive zone (CZ) elements have been designed and introduced to FEM so that the CZ-FEM can capture the cracks. However, they should be placed where the crack is anticipated to occur. In other words, CZ-FEM requires predefined crack path. So, this method cannot be used for a brittle cutting simulation due to the complex nature of the process and unpredictable fracture and cracks.
7. This study proposed a fracture-based finite element method, named Embedded Cohesive Zone Finite Element Method (ECZ-FEM), to model brittle materials cutting. In ECZ-FEM, a network of cohesive zone (CZ) elements is embedded in the material body to capture undetermined crack initiation and propagation during a cutting process.
8. In ECZ-FEM, the maximum deflection of the CZ element should be limited by a scaling factor to control the material ductility and chip formation. Different scaling factors might generate different chip formations. To

obtain an appropriate scaling factor, the model should be calibrated against the experiment.

9. Comparing the numerical results against the experiment demonstrates that ECZ-FEM can capture dusty debris, irregular chips, and unstable crack propagation as expected for brittle materials cutting. However, it overstimates the cutting forces by 30-50%.
10. ECZ-FEM has demonstrated the applicability to brittle materials that are rigid and have no plastic deformation.

6.2. Future work

The models proposed in this study can be further improved and /or extended in the following directions:

1. The main goal of this study was to understand the mechanics of brittle materials cutting. So, the selected brittle material was assumed to be isotropic, and temperature and strains rate independent. The effects of anisotropic, temperature and strain rate dependent materials can also be investigated.
2. The models applied to an orthogonal cutting process which is the most basic configuration of machining processes. The models can be extended to a 3D configuration such as drilling.
3. For applying SPH to brittle materials cutting, to achieve higher accuracy and resolve the numerical instabilities, the algorithm itself can be improved

by adopting renormalization formulation or setting “ghost” particles around the boundaries.

4. In ECZ-FEM, the CZ elements behavior including the traction-deflection relationship can be customized due to the fact that by embedding the CZ elements all around a main element, they have to share several nodes and it might affect the overall behavior of the elements.

REFERENCES

[1] D. Stephenson, Surface integrity control during the precision machining of brittle materials, ADVANCES IN TECHNOLOGY OF MATERIALS AND MATERIALS PROCESSING JOURNAL, 8 (2006) 13.

[2] M.C. Shaw, J. Cookson, Metal cutting principles, Clarendon press Oxford, 1984.

[3] B. Takabi, M. Tajdari, B.L. Tai, Numerical study of smoothed particle hydrodynamics method in orthogonal cutting simulations–Effects of damage criteria and particle density, Journal of Manufacturing Processes, 30 (2017) 523-531.

[4] X. Geng, W. Dou, J. Deng, F. Ji, Z. Yue, Simulation of the orthogonal cutting of OFHC copper based on the smoothed particle hydrodynamics method, The International Journal of Advanced Manufacturing Technology, 91 (2017) 265-272.

[5] D. Che, W.-L. Zhu, K.F. Ehmann, Chipping and crushing mechanisms in orthogonal rock cutting, International Journal of Mechanical Sciences, 119 (2016) 224-236.

[6] B. Takabi, B.L. Tai, A review of cutting mechanics and modeling techniques for biological materials, Medical Engineering and Physics, 45 (2017) 1-14.

[7] M. Marco, M. Rodríguez-Millán, C. Santiuste, E. Giner, M.H. Miguélez, A review on recent advances in numerical modelling of bone cutting, Journal of the mechanical behavior of biomedical materials, 44 (2015) 179-201.

[8] E. Uhlmann, M.G. von der Schulenburg, R. Zettier, Finite element modeling and cutting simulation of Inconel 718, CIRP Annals-Manufacturing Technology, 56 (2007) 61-64.

[9] S. Soo, D. Aspinwall, R. Dewes, 3D FE modelling of the cutting of Inconel 718, Journal of Materials Processing Technology, 150 (2004) 116-123.

[10] K. Alam, A. Mitrofanov, M. Bäker, V. Silberschmidt, Temperature Calculations in Orthogonal Cutting of Cortical Bone Using Finite Element Analysis, in: 25th Southern Biomedical Engineering Conference 2009, 15–17 May 2009, Miami, Florida, USA, Springer, 2009, pp. 151-152.

[11] A. Molinari, R. Cheriguene, H. Miguelez, Contact variables and thermal effects at the tool–chip interface in orthogonal cutting, International journal of Solids and Structures, 49 (2012) 3774-3796.

[12] E. Ceretti, P. Fallböhmer, W. Wu, T. Altan, Application of 2D FEM to chip formation in orthogonal cutting, Journal of Materials Processing Technology, 59 (1996) 169-180.

[13] E. Ceretti, M. Lucchi, T. Altan, FEM simulation of orthogonal cutting: serrated chip formation, Journal of Materials Processing Technology, 95 (1999) 17-26.

[14] F. Klocke, H.-W. Raedt, S. Hoppe, 2D-FEM simulation of the orthogonal high speed cutting process, (2001).

[15] K. Saanouni, P. Lestriez, C. Labergère, 2D adaptive FE simulations in finite thermo-elasto-viscoplasticity with ductile damage: application to orthogonal metal cutting by chip formation and breaking, International Journal of Damage Mechanics, 20 (2011) 23-61.

[16] A. Mamalis, M. Horvath, A. Branis, D. Manolakos, Finite element simulation of chip formation in orthogonal metal cutting, Journal of Materials Processing Technology, 110 (2001) 19-27.

[17] F. Klocke, D. Lung, S. Buchkremer, Inverse identification of the constitutive equation of Inconel 718 and AISI 1045 from FE machining simulations, Procedia CIRP, 8 (2013) 212-217.

[18] K. Alam, A. Mitrofanov, V.V. Silberschmidt, Finite element analysis of forces of plane cutting of cortical bone, Computational Materials Science, 46 (2009) 738-743.

[19] A. Ramesh, S.N. Melkote, Modeling of white layer formation under thermally dominant conditions in orthogonal machining of hardened AISI 52100 steel, International Journal of Machine Tools and Manufacture, 48 (2008) 402-414.

[20] C. Duan, T. Dou, Y. Cai, Y. Li, Finite element simulation and experiment of chip formation process during high speed machining of AISI 1045 hardened steel, International Journal of Recent Trends in Engineering, 1 (2009) 46-50.

[21] J. Outeiro, D. Umbrello, R. M'saoubi, Experimental and numerical modelling of the residual stresses induced in orthogonal cutting of AISI 316L steel, International Journal of Machine Tools and Manufacture, 46 (2006) 1786-1794.

[22] D. Umbrello, R. M'saoubi, J. Outeiro, The influence of Johnson–Cook material constants on finite element simulation of machining of AISI 316L steel, International Journal of Machine Tools and Manufacture, 47 (2007) 462-470.

[23] A. Mitrofanov, V. Babitsky, V. Silberschmidt, Finite element analysis of ultrasonically assisted turning of Inconel 718, Journal of materials processing technology, 153 (2004) 233-239.

[24] N. Ahmed, A. Mitrofanov, V. Babitsky, V. Silberschmidt, Analysis of forces in ultrasonically assisted turning, Journal of Sound and Vibration, 308 (2007) 845-854.

[25] K. Alam, A. Mitrofanov, V.V. Silberschmidt, Thermal analysis of orthogonal cutting of cortical bone using finite element simulations, International Journal of Experimental and Computational Biomechanics, 1 (2010) 236-251.

[26] S.R. Davidson, D.F. James, Drilling in bone: modeling heat generation and temperature distribution, Journal of biomechanical engineering, 125 (2003) 305-314.

[27] R. Huiskes, Some fundamental aspects of human joint replacement: analyses of stresses and heat conduction in bone-prosthesis structures, Acta Orthopaedica Scandinavica, 51 (1980) 3-208.

[28] K. Alam, A. Ghafoor, V.V. Silberschmidt, Analysis of forces and temperatures in conventional and ultrasonically-assisted cutting of bone, in: Advanced Materials Research, Trans Tech Publ, 2011, pp. 247-254.

[29] T. Childs, D. Arola, Machining of cortical bone: Simulations of chip formation mechanics using metal machining models, Machining Science and Technology, 15 (2011) 206-230.

[30] D.T. REILLY, A.H. BURSTEIN, The mechanical properties of cortical bone, J Bone Joint Surg Am, 56 (1974) 1001-1022.

[31] D.C. Drucker, W. Prager, Soil mechanics and plastic analysis or limit design, Quarterly of applied mathematics, 10 (1952) 157-165.

[32] C. Santiuste, M. Rodríguez-Millán, E. Giner, H. Miguélez, The influence of anisotropy in numerical modeling of orthogonal cutting of cortical bone, Composite Structures, 116 (2014) 423-431.

[33] J. Hou, N. Petrinic, C. Ruiz, S. Hallett, Prediction of impact damage in composite plates, Composites Science and Technology, 60 (2000) 273-281.

[34] J. Limido, C. Espinosa, M. Salaun, C. Mabru, R. Chieragatti, J.-L. Lacome, Metal cutting modelling SPH approach, International journal of machining and machinability of materials, 9 (2011) 177-196.

[35] J. Limido, C. Espinosa, M. Salaun, J.-L. Lacome, A new approach of high speed cutting modelling: SPH method, in: Journal de Physique IV (Proceedings), EDP sciences, 2006, pp. 1195-1200.

[36] M. Madaj, M. Píška, On the SPH orthogonal cutting simulation of A2024-T351 alloy, Procedia CIRP, 8 (2013) 152-157.

[37] J. Dănuț, SPH meshless simulation of orthogonal cutting of AA6060-T6, in: Applied Mechanics and Materials, Trans Tech Publ, 2015, pp. 258-263.

[38] J. Limido, C. Espinosa, M. Salaün, J.-L. Lacome, SPH method applied to high speed cutting modelling, International journal of mechanical sciences, 49 (2007) 898-908.

[39] M.F. Villumsen, T.G. Fauerholdt, Simulation of metal cutting using smooth particle hydrodynamics, Tagungsberichtsband Zum-DYNA Anwenderforum Bamb, 30 (2008).

[40] S. Li, A. Abdel-Wahab, E. Demirci, V.V. Silberschmidt, Penetration of cutting tool into cortical bone: experimental and numerical investigation of anisotropic mechanical behaviour, Journal of biomechanics, 47 (2014) 1117-1126.

[41] K. Alam, A. Mitrofanov, M. Bäker, V. Silberschmidt, Stresses in ultrasonically assisted bone cutting, in: Journal of Physics: Conference Series, IOP Publishing, 2009, pp. 012014.

[42] S. Li, E. Demirci, V.V. Silberschmidt, Variability and anisotropy of mechanical behavior of cortical bone in tension and compression, Journal of the mechanical behavior of biomedical materials, 21 (2013) 109-120.

[43] M. Tajdari, B.L. Tai, Modeling of Brittle and Ductile Materials Drilling Using Smoothed-Particle Hydrodynamics, in: ASME 2016 11th International Manufacturing Science and Engineering Conference, American Society of Mechanical Engineers, 2016, pp. V002T003A013-V002T003A013.

[44] D. Arola, M. Sultan, M. Ramulu, Finite element modeling of edge trimming fiber reinforced plastics, Journal of manufacturing science and engineering, 124 (2002) 32-41.

[45] R. Zitoune, F. Collombet, F. Lachaud, R. Piquet, P. Pasquet, Experiment–calculation comparison of the cutting conditions representative of the long fiber composite drilling phase, Composites Science and Technology, 65 (2005) 455-466.

[46] Y. Tian, Y.C. Shin, Multiscale finite element modeling of silicon nitride ceramics undergoing laser-assisted machining, Journal of Manufacturing Science and Engineering, 129 (2007) 287-295.

[47] X. Dong, Y.C. Shin, Multi-scale genome modeling for predicting fracture strength of silicon carbide ceramics, Computational Materials Science, 141 (2018) 10-18.

[48] C.R. Dandekar, Y.C. Shin, Multi-scale modeling to predict sub-surface damage applied to laser-assisted machining of a particulate reinforced metal matrix composite, Journal of Materials Processing Technology, 213 (2013) 153-160.

[49] G.V.G. Rao, P. Mahajan, N. Bhatnagar, Micro-mechanical modeling of machining of FRP composites–Cutting force analysis, Composites science and technology, 67 (2007) 579-593.

[50] S. Usui, J. Wadell, T. Marusich, Finite element modeling of carbon fiber composite orthogonal cutting and drilling, Procedia CIRP, 14 (2014) 211-216.

[51] J. Xu, M. El Mansori, Cutting modeling using cohesive zone concept of titanium/CFRP composite stacks, International Journal of Precision Engineering and Manufacturing, 16 (2015) 2091-2100.

[52] M.C. Shaw, Metal cutting principles, Oxford university press New York, 2005.

[53] P.N. Blake, R.O. Scattergood, Ductile- Regime Machining of Germanium and Silicon, Journal of the American ceramic society, 73 (1990) 949-957.

[54] O. Su, N.A. Akcin, Numerical simulation of rock cutting using the discrete element method, International Journal of Rock Mechanics and Mining Sciences, 48 (2011) 434-442.

[55] S.F. Malak, I.A. Anderson, Orthogonal cutting of cancellous bone with application to the harvesting of bone autograft, Medical engineering & physics, 30 (2008) 717-724.

[56] P. Krasauskas, S. Kilikevičius, R. Česnavičius, D. Pačenga, Experimental analysis and numerical simulation of the stainless AISI 304 steel friction drilling process, Mechanics, 20 (2015) 590-595.

[57] W.A. Lughmani, K. Bouazza-Marouf, I. Ashcroft, Drilling in cortical bone: a finite element model and experimental investigations, journal of the mechanical behavior of biomedical materials, 42 (2015) 32-42.

[58] A.J. Shih, Finite element simulation of orthogonal metal cutting, TRANSACTIONS-AMERICAN SOCIETY OF MECHANICAL ENGINEERS JOURNAL OF ENGINEERING FOR INDUSTRY, 117 (1995) 84-84.

[59] M. Bäker, Finite element simulation of high-speed cutting forces, Journal of Materials Processing Technology, 176 (2006) 117-126.

[60] T. Marusich, S. Usui, J. Ma, D. Stephenson, A. Shih, Finite element modeling of drilling processes with solid and indexable tooling in metals and stack-ups, (2007).

[61] B. Rao, Y.C. Shin, Analysis on high-speed face-milling of 7075-T6 aluminum using carbide and diamond cutters, International Journal of Machine Tools and Manufacture, 41 (2001) 1763-1781.

[62] M. Elhachimi, S. Torbaty, P. Joyot, Mechanical modelling of high speed drilling. 1: predicting torque and thrust, International Journal of Machine Tools and Manufacture, 39 (1999) 553-568.

[63] M. Calamaz, J. Limido, M. Nouari, C. Espinosa, D. Coupard, M. Salaün, F. Girot, R. Chieragatti, Toward a better understanding of tool wear effect through a comparison between experiments and SPH numerical modelling of machining hard materials, International journal of refractory metals and hard materials, 27 (2009) 595-604.

[64] J.J. Monaghan, Smoothed particle hydrodynamics, Reports on progress in physics, 68 (2005) 1703.

[65] R. Williams, A study of the drilling process, ASME J. Eng. Ind, 96 (1974) 1207-1215.

[66] A. Nassiri, B. Kinsey, Numerical studies on high-velocity impact welding: smoothed particle hydrodynamics (SPH) and arbitrary Lagrangian–Eulerian (ALE), Journal of Manufacturing Processes, 24 (2016) 376-381.

[67] Y. Aizawa, J. Nishiwaki, Y. Harada, S. Muraishi, S. Kumai, Experimental and numerical analysis of the formation behavior of intermediate layers at explosive welded Al/Fe joint interfaces, Journal of Manufacturing Processes, 24 (2016) 100-106.

[68] F. Spreng, P. Eberhard, Machining Process Simulations with Smoothed Particle Hydrodynamics, Procedia CIRP, 31 (2015) 94-99.

[69] U. Umer, M.K. Mohammed, J.A. Qudeiri, A. Al-Ahmari, Assessment of finite element and smoothed particles hydrodynamics methods for modeling serrated chip formation in hardened steel, Advances in Mechanical Engineering, 8 (2016) 1687814016652372.

[70] B. Takabi, B.L. Tai, A review of cutting mechanics and modeling techniques for biological materials, Medical Engineering & Physics, (2017).

[71] J. Liu, Y. Bai, C. Xu, Evaluation of ductile fracture models in finite element simulation of metal cutting processes, Journal of Manufacturing Science and Engineering, 136 (2014) 011010.

[72] T. Mabrouki, F. Girardin, M. Asad, J.-F. Rigal, Numerical and experimental study of dry cutting for an aeronautic aluminium alloy (A2024-T351), International Journal of Machine Tools and Manufacture, 48 (2008) 1187-1197.

[73] K. Alam, M. Khan, V.V. Silberschmidt, 3D Finite-Element Modelling of Drilling Cortical Bone: Temperature Analysis, J Med Biol Eng, 34 (2014) 618-623.

[74] G. Augustin, T. Zigman, S. Davila, T. Udilljak, T. Staroveski, D. Brezak, S. Babic, Cortical bone drilling and thermal osteonecrosis, Clinical biomechanics, 27 (2012) 313-325.

[75] R.K. Pandey, S. Panda, Drilling of bone: A comprehensive review, Journal of clinical orthopaedics and trauma, 4 (2013) 15-30.

[76] S. Diehl, G. Rockefeller, C.L. Fryer, D. Riethmiller, T.S. Statler, Generating Optimal Initial Conditions for Smoothed Particle Hydrodynamics Simulations, Publications of the Astronomical Society of Australia, 32 (2015) e048.

[77] S. Li, W.K. Liu, Meshfree particle methods, Springer Science & Business Media, 2007.

[78] J.J. Monaghan, Smoothed particle hydrodynamics, Annual review of astronomy and astrophysics, 30 (1992) 543-574.

[79] V. Abaqus, 6.14 Documentation, Dassault Systemes Simulia Corporation, (2014).

[80] C. Espinosa, J. Lacome, J. Limido, M. Salaun, C. Mabru, R. Chieragatti, Modeling high speed machining with the SPH method, in: 10th International LS-DYNA users conference, 2008.

[81] J. Strenkowski, K.-J. Moon, Finite element prediction of chip geometry and tool/workpiece temperature distributions in orthogonal metal cutting, Journal of Engineering for Industry, 112 (1990) 313-318.

[82] R. Smerd, S. Winkler, C. Salisbury, M. Worswick, D. Lloyd, M. Finn, High strain rate tensile testing of automotive aluminum alloy sheet, International Journal of Impact Engineering, 32 (2005) 541-560.

[83] Y. Guo, D.W. Yen, A FEM study on mechanisms of discontinuous chip formation in hard machining, Journal of Materials Processing Technology, 155 (2004) 1350-1356.

[84] N. Gupta, M. Iqbal, G. Sekhon, Experimental and numerical studies on the behavior of thin aluminum plates subjected to impact by blunt-and hemispherical-nosed projectiles, International Journal of Impact Engineering, 32 (2006) 1921-1944.

[85] V. Balden, G. Nurick, Numerical simulation of the post-failure motion of steel plates subjected to blast loading, International Journal of Impact Engineering, 32 (2005) 14-34.

[86] M. Barge, H. Hamdi, J. Rech, J.-M. Bergheau, Numerical modelling of orthogonal cutting: influence of numerical parameters, Journal of Materials Processing Technology, 164 (2005) 1148-1153.

[87] H. Sadeghinia, M. Razfar, J. Takabi, 2D finite element modeling of face milling with damage effects, in: 3rd WSEAS international conference on applied and theoretical mechanics, Spain, 2007.

[88] W. Zhang, S.A. Tekalur, M. Baumann, L.R. McCabe, The effects of damage accumulation on the tensile strength and toughness of compact bovine bone, Journal of biomechanics, 46 (2013) 964-972.

[89] J. Phelps, G. Hubbard, X. Wang, C. Agrawal, Microstructural heterogeneity and the fracture toughness of bone, Journal of biomedical materials research, 51 (2000) 735-741.

[90] G. Chen, J. Li, Y. He, C. Ren, A new approach to the determination of plastic flow stress and failure initiation strain for aluminum alloys cutting process, Computational Materials Science, 95 (2014) 568-578.

[91] C. Yeager, A. Nazari, D. Arola, Machining of cortical bone: surface texture, surface integrity and cutting forces, Machining Science and Technology, 12 (2008) 100-118.

[92] Y. Xi, M. Bermingham, G. Wang, M. Dargusch, SPH/FE modeling of cutting force and chip formation during thermally assisted machining of Ti6Al4V alloy, Computational materials science, 84 (2014) 188-197.

[93] M. Liu, G. Liu, Smoothed particle hydrodynamics (SPH): an overview and recent developments, Archives of computational methods in engineering, 17 (2010) 25-76.

[94] T. Belytschko, S. Xiao, Stability analysis of particle methods with corrected derivatives, Computers & Mathematics with Applications, 43 (2002) 329-350.

[95] D. Liu, W. Cong, Z.J. Pei, Y. Tang, A cutting force model for rotary ultrasonic machining of brittle materials, International Journal of Machine Tools and Manufacture, 52 (2012) 77-84.

[96] U. Umer, M. Ashfaq, J. Qudeiri, H. Hussein, S. Danish, A. Al-Ahmari, Modeling machining of particle-reinforced aluminum-based metal matrix composites using cohesive zone elements, The International Journal of Advanced Manufacturing Technology, 78 (2015) 1171-1179.

[97] C. Santiuste, X. Soldani, M.H. Miguélez, Machining FEM model of long fiber composites for aeronautical components, Composite structures, 92 (2010) 691-698.

[98] A. Shrot, M. Bäker, Determination of Johnson–Cook parameters from machining simulations, Computational Materials Science, 52 (2012) 298-304.

[99] J. Shi, C.R. Liu, The influence of material models on finite element simulation of machining, Journal of manufacturing science and engineering, 126 (2004) 849-857.

[100] A. Turon, C.G. Davila, P.P. Camanho, J. Costa, An engineering solution for mesh size effects in the simulation of delamination using cohesive zone models, Engineering fracture mechanics, 74 (2007) 1665-1682.

[101] G. Paulino, Z. Zhang, Cohesive modeling of propagating cracks in homogeneous and functionally graded composites, in: 5th GRACM International Congress on Computational Mechanics, 2005.

[102] P. Oxley, Shear angle solutions in orthogonal machining, International Journal of Machine Tool Design and Research, 2 (1962) 219-229.

[103] H.D. Espinosa, P.D. Zavattieri, A grain level model for the study of failure initiation and evolution in polycrystalline brittle materials. Part II: numerical examples, Mechanics of Materials, 35 (2003) 365-394.

[104] D.S.S. Corp, Selecting Material Parameters in Abaqus for Cohesive Elements Defined in Terms Of Traction-Separation

[105] H. Bil, S.E. Kılıç, A.E. Tekkaya, A comparison of orthogonal cutting data from experiments with three different finite element models, International Journal of Machine Tools and Manufacture, 44 (2004) 933-944.

[106] K. Iwata, K. Osakada, Y. Terasaka, Process modeling of orthogonal cutting by the rigid-plastic finite element method, Journal of Engineering Materials and Technology, 106 (1984) 132-138.

[107] A. Molinari, C. Musquar, G. Sutter, Adiabatic shear banding in high speed machining of Ti–6Al–4V: experiments and modeling, International journal of Plasticity, 18 (2002) 443-459.

[108] F. Chegdani, B. Takabi, B.L. Tai, M. El Mansori, S.T. Bukkapatnam, Thermal Effects on Tribological Behavior in Machining Natural Fiber Composites, Procedia Manufacturing, 26 (2018) 305-316.

[109] D.o.P.R.L. Sawbones, Inc, Washington. , in, 2013.

[110] L. Marsavina, D.M. Constantinescu, E. Linul, D.A. Apostol, T. Voiconi, T. Sadowski, Refinements on fracture toughness of PUR foams, Engineering Fracture Mechanics, 129 (2014) 54-66.

[111] T. Kobayashi, I. Yamamoto, M. Niinomi, Introduction of a new dynamic fracture toughness evaluation system, Journal of Testing and Evaluation, 21 (1993) 145-153.

[112] A. Kobayashi, S. Mall, Dynamic fracture toughness of Homalite-100, Experimental Mechanics, 18 (1978) 11-18.